



**School of Chemistry**

**Nanodiamond Hydrogel:  
A New Class of Material**

**Alexander Dennehy**

**Supervisor: Dr. W. Briscoe**

**Second Assessor: Prof. P. May**

This work is submitted in partial fulfilment of the requirements for the  
Honours Degree of MSci Chemistry at the University of Bristol.

## Abstract

Owing to its remarkable array of desirable chemical and physical characteristics, nanodiamond is considered an ideal component for composite material design. As such numerous examples of non-covalently bound nanodiamond composites have been reported in the literature, the majority of which were prepared by simple admixing of the nanodiamond during polymerisation. Conversely, covalently bound nanodiamond composites have been studied to a far less extent, possibly due to the complexity of design. Thus, upon recognising the need for further exploration in this field, it was decided that the premise of this work would be to devise a method for synthesising a whole new class of composite material, one in which an array of functionalised nanodiamond particles would be covalently incorporated within a three dimensional polymer matrix. This would constitute the so-called nanodiamond hydrogel and to our knowledge would be the first of its kind reported in the literature. The properties exhibited by the novel composite will be of great interest, with a particular emphasis on its potential applications.

Synthesis of the nanodiamond hydrogel was pursued by means of atom transfer radical polymerisation (ATRP), a type of addition polymerisation. This required a homogeneous surface functionalisation of the nanodiamond,  $d = 50$  nm, thus a preliminary characterisation of the surface functionality of the nanodiamond starting material was first required, this was achieved using Fourier transform infrared spectroscopy (FTIR), elemental analysis (EA) and X-ray powder diffraction (XRD). These techniques were indicative of a dense covering of oxygen containing groups on the surface, along with a thin coating of graphite. Thus, to ensure a complete homogenisation of the surface functionality, the nanodiamond was treated with piranha solution, a 3:1 mixture of  $H_2SO_4$  and  $H_2O_2$ . It was expected that this would result in removal of the graphite from the surface and an increase in the abundance of surface hydroxyl groups, this was again confirmed using FTIR, EA and XRD. However, in order to facilitate ATRP, surface chlorination was also required. This was achieved using by reacting the hydroxyl groups on the surface with the initiator, 2-chloropropionyl chloride. Successful chlorination was confirmed via FTIR and EA.

A series of ATRP reactions was then performed using the chlorinated nanodiamond, and the monomer, poly (ethylene) glycol methyl ether methacrylate. A loading of 20 mg for the nanodiamond was found to be most effective. Synthesis of the nanodiamond hydrogels was then repeated in the presence of the cross-linker, ethylene glycol dimethacrylate. A quantitative analysis of the mechanical properties of the nanodiamond hydrogels was then carried out using a series of rheological tests. The elastic modulus was greatest for those gels prepared using the highest ratio of monomer to cross-linker as expected, it was also lower for those gels that had undergone covalent incorporation of the nanodiamond, contrary to our initial prediction.

## **Acknowledgements**

First and foremost I would like to thank my supervisor Dr. Wuge Briscoe for all of his guidance and support throughout the duration of the project. I would also to thank my second assessor, Prof. Paul May, for his valuable contribution during the development stage of the work and for his assistance with Raman spectroscopy. Similarly, I would like to express my deepest thanks to Mr. Tim Snow, whose technical expertise and academic contribution throughout was tremendously helpful. His willingness to give his time so generously was very much appreciated.

My thanks are also extended to Mr. Christian Redeker and Mr. Lee Hall for their assistance in carrying out X-ray powder diffraction, to Dr. Cheryl Flynn of the Bristol Colloids Group for her assistance with all of the rheological measurements and to Ms. Charlotte Beddoes for her proof reading. On a final note, I would like to thank the entire Briscoe Group for making the year so memorable.

# Contents

Abstract .....	i
Acknowledgements .....	ii
1. Introduction .....	1
1.1. Nanodiamond.....	1
1.1.1. Nanodiamond Discovery .....	1
1.1.2. Nanodiamond Preparation .....	2
1.1.3. Structure of Nanodiamond .....	5
1.1.4. Properties of Nanodiamond .....	7
1.1.5. Nanodiamond Surface Functionalisation.....	11
1.1.6. Nanodiamond Composites.....	14
1.2. Hydrogels.....	15
1.2.1. Hydrogel Classification.....	15
1.2.2. Hydrogel Properties .....	17
1.2.3. Mechanisms of Hydrogel Formation.....	18
1.2.4. Atom Transfer Radical Polymerisation.....	18
1.2.5. Hydrogel Applications .....	19
1.3. Nanodiamond Hydrogels .....	20
1.3.1. Strategy for Synthesis .....	21
1.3.2. Nanodiamond Hydrogel Applications .....	22
1.4. Characterisation.....	23
1.4.1. Fourier Transform Infrared Spectroscopy.....	23
1.4.2. Raman Spectroscopy .....	24
1.4.3. X-Ray Powder Diffraction.....	24
1.4.4. Scanning Electron Microscopy .....	24
1.4.5. Transmission Electron Microscopy.....	25
1.4.6. Dynamic Light Scattering .....	25
1.4.7. Rheological Tests .....	25
2. Experimental .....	26
2.1. Preparation and Characterisation of the Nanodiamond Starting Material.....	26
2.2. Nanodiamond Surface Oxidation.....	26
2.3. Nanodiamond Surface Chlorination .....	27
2.4. Nanodiamond Hydrogel Synthesis.....	28
2.4.1. Absence of Cross-Linker .....	28
2.4.2. Presence of Cross-Linker.....	29

2.5. Rheological Measurements of Hydrogels.....	30
3. Results and Discussion.....	31
3.1. Characterisation of the Nanodiamond Starting Material.....	31
3.1.1. Surface Functionality .....	31
3.1.2. Size.....	34
3.2. The Effects of Surface Oxidation .....	35
3.2.1 Surface Functionality .....	35
3.2.2. Size.....	38
3.3. The Effects of Surface Chlorination .....	39
3.3.1. Surface Functionality .....	40
3.3.2. Size.....	41
3.4. Nanodiamond Hydrogel Synthesis.....	42
3.4.1. Absence of Cross-Linker .....	44
3.4.2. Presence of Cross-Linker.....	48
3.5. Rheology of the Hydrogels.....	49
3.5.1. The Effect of Adding the Cross-linker.....	50
3.5.2. The Effect of Adding the Nanodiamond.....	51
4. Conclusions .....	52
5. Future Study .....	52
5.1. The Effect of Nanodiamond Loading.....	52
5.2. The Effects of Surface Functionalisation .....	53
5.3. Further Characterisation.....	53
6. References .....	53

# **1. Introduction**

## **1.1. Nanodiamond**

Within the last five years the field of nanodiamond research has experienced unprecedented growth, largely owing to the recent discovery of a unique array of remarkable chemical and physical characteristics of this material [1]. Properties of particular interest include the material's excellent biocompatibility, tuneable surface chemistry, high mechanical strength and stable luminescence, all of which suggest nanodiamond has great potential in the field of composite materials research.

### **1.1.1. Nanodiamond Discovery**

Nanodiamond has taken centre stage within the last couple of years and as such one might assume the origins of this material are comparatively recent [1]. The first case of successful nanodiamond synthesis however, was reported in 1959, when two American scientists, De Carli and Jamieson, observed the formation of tiny diamond crystallites upon the action of a shockwave on graphite [2]. This method of synthesis would later be known as 'shockwave synthesis', and go on to become one of the most effective methods of synthesising nanodiamond on an industrial scale [3].

An alternative method of nanodiamond synthesis was also pioneered by two Russian chemists, Volkov and Danilenko, soon after De Carli and Jamieson's initial discovery. The new method became known as 'detonation synthesis' as the Russian pair had observed traces of nanodiamond in the soot generated by the detonation of a carbonaceous explosive [4]. Their work remained unpublished however, as it was carried out during the Cold War and the field of nanodiamond research quickly stagnated, an example of how the progression of science can be thwarted by politics [3]. It was then only after the fall of communism in the late 1980s that the release of Volkov and Danilenko's innovative work caused a resurgence in the field of nanodiamond research.

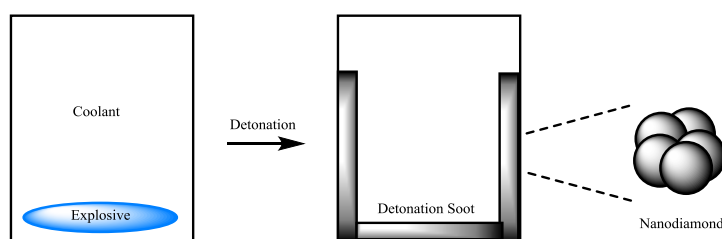
The first plant for the industrial scale production of detonation nanodiamond was opened in the early nineties bringing the capacity to produce nanodiamond on the industrial scale at a low cost [4]. It was this that gave nanodiamond research an edge over other nanoscale carbon materials.

### 1.1.2. Nanodiamond Preparation

Both methods used to synthesise nanodiamond on an industrial scale, i.e. detonation and shockwave synthesis, require high temperature and pressure, as it only in this region of carbon's phase diagram that diamond is thermodynamically stable.

#### 1.1.2.1. Detonation Synthesis

Detonation synthesis involves the detonation of a carbonaceous explosive in a confined container to generate sufficient pressures to convert carbon into nanodiamond, see Scheme 1.



**Scheme 1:** Detonation synthesis of nanodiamond.

In principle there are two methods of detonation synthesis; both are remarkably similar, differing only by the choice of starting material [3]. The first method requires the use of two starting materials, the explosive and some form of graphite. Upon detonation, two processes occur simultaneously; the first involves direct conversion of the already existing elemental carbon, the second involves condensation of carbon from the explosive. Both result in nanodiamond formation. Different particles are obtained depending on the ambient conditions. Conducting the reaction in an inert gas leads to the exclusive formation of cubic diamond with the primary particles measuring approximately 20 nm, when performed in air, on the other hand, particle size diminishes to 8 nm and prevalence of hexagonal diamond (*Lonsdaleite*) increases [2].

The second method requires the use of only one starting material, i.e. the explosive, which serves both as a source of energy and carbon. Initially, trinitrotoluene (TNT) was thought to be the most suitable explosive as pressures of ca. 18 GPa and temperatures up to 3500 °C are achieved upon its detonation [3]. These conditions correspond directly to the region of the carbon phase diagram where diamond is the most thermodynamically stable allotrope. Furthermore, TNT is relatively cheap and readily available compared to other explosives. However, the soot obtained from the detonation of pure TNT is found to contain just 15 % of diamond-like carbon [5]. This is because TNT has a comparatively low content of energy, so the shock wave formed is relatively weak. To resolve this problem, energetic mixed explosives such as 'hexolite' are employed, these possess a

typical composition of TNT and hexogen in a 2:3 ratio, see Figures 1 and 2 respectively. The use of hexogen alone is unfeasible, as it is found that just 1 % of its carbon remains as diamond after detonation. This is due to hexogen's poor negative oxygen balance, which results in the majority of the carbon found in the explosive being lost as oxidised gases, i.e. CO<sub>2</sub> or CO [3]. A mixture of TNT and hexogen is therefore ideal, as the soot-forming properties of TNT and high energy content of hexogen complement each other well, resulting in up to 10 % of the available carbon being isolated as detonation soot [5]. More importantly, approximately 60 – 80 % of this detonation soot is found to be nanoscale diamond [2].

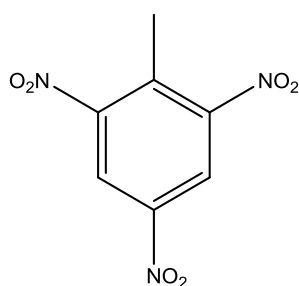


**Figure 1:** TNT

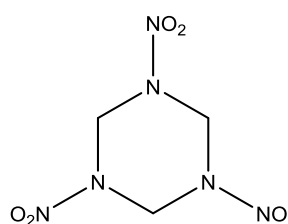


**Figure 2:** Hexogen

The mechanism behind nanodiamond formation is well understood, beginning with the release of carbon atoms from the decomposition of the explosive. These atoms then coalesce to form small diamond clusters, which continue to grow by diffusion under the high pressure generated by the explosion. Growth rapidly ceases when the pressure subsides, in turn, the time window for diamond formation is prohibitively narrow, thus limiting the size of the particles to a few hundred nanometres. Temperature is far slower to decline however, resulting in continued graphite formation long after the initial shockwave causing the sp<sup>2</sup> hybridised carbon to deposit either as a shell on the pre-existing diamond cores or as loose clusters. Therefore to prevent contamination of the nanodiamond with the graphitic impurity, an efficient method of cooling is required, i.e. to cross the critical temperature for graphite formation as rapidly as possible [3].

Two types of coolant are used for detonation synthesis, inert gases or liquids, examples of the former include; CO<sub>2</sub>, N<sub>2</sub> or even air. The use of inert gases can often be preferable, as they participate in very few side reactions with the nanodiamond surface. A drawback however is poor heat capacity, limiting the rate of cooling thus increasing the amount of graphite deposited on the nanodiamond surface. Therefore, a liquid coolant such as water is used when rapid cooling is required, the drawback now being a tendency to result in a strong functionalisation of the nanodiamonds surface. Functionalisation ensues because the conditions prevailing in the reactor, i.e. high temperature and pressure, cause the water to become supercritical and thus highly

reactive. As a result the surface of the nanodiamond can often be dominated by an array of oxygen containing groups, i.e. carboxyl, hydroxyl and keto groups [5].

### 1.1.2.2. Shockwave Synthesis

Instead of adopting a detonation technique to achieve the high pressures desired, external shockwaves can also be employed in the synthesis of nanodiamonds. First pioneered by De Carli and Jamieson in the early 1960s [2], this method of synthesis is now employed by the DuPont Corp. to yield 2 million karat of nanoscale diamond industrially each year [3]. These nanodiamonds are typically processed by sintering to give durable cutting and polishing tools.

Extremely pure synthetic graphite is placed in a sealed metal contained which is surrounded by another, thicker, metal tube, see Figure 3. This assembly is placed in a reactor where the outer tube is filled with an explosive and the charge lit at one end. The resultant circular shockwave then runs down the inner metal tube, which is compressed by the action of the pressure, transferring the pressure onto the graphitic material inside. Pressures achieved typically surpass 48 GPa, resulting in the formation of primary nanodiamond particles with a diameter between 10 and 20 nm [3]. As with detonation synthesis, the pressure inside the reaction tube drops much more rapidly than the temperature, resulting in considerable losses to the final yield as reversion into graphite is promoted. Depending on the specific method involved, the final yield of nanodiamond can be anywhere between 10 and 25 % [3]. Unlike detonation synthesis, the mechanism of shockwave induced conversion has yet to be fully elucidated.

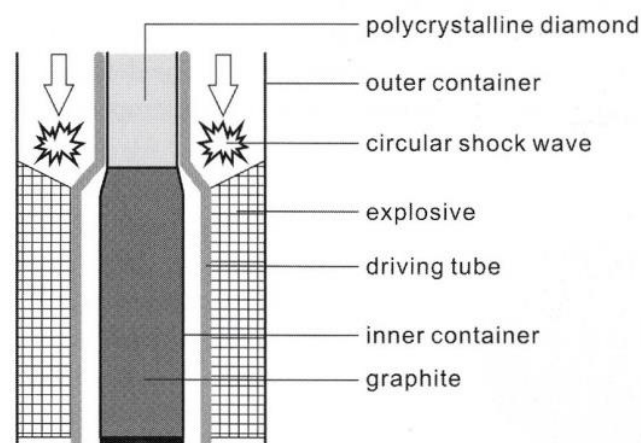


**Figure 3:** Reactor used in shockwave synthesis of nanodiamond. [3]

### 1.1.3. Structure of Nanodiamond

#### 1.1.3.1. Lattice Structure

The lattice structure of nanodiamond corresponds with that of the bulk material in all essential features, with each  $sp^3$  hybridised carbon atom bonded to four adjacent atoms in a regularly repeating tetrahedral structure. The bond length throughout the lattice is also uniform, identical to that of the bulk material, i.e. 154.45 pm, with both cubic and hexagonal variants of the diamond structure having been observed, see Figure 4 for the cubic structure. The lattice constant for the nanoscale material differs just slightly from the value of 2.456 Å recorded for bulk diamond as determined by X-ray diffraction [3].

Despite these similarities, there are some notable differences between the lattice structures of the two materials, primarily, the altered bond strain exhibited close to the surface of the nanoscale material. This arises due to the large portion of surface atoms that cause strain within the particles. In NMR examinations, for instance, the carbon atoms on the surface exhibit an additional chemical shift compared to those situated in the core. This is due to the presence of  $sp^2$  hybridised carbon on the surface.

In addition, lattice defects are also more prevalent in the nanoscale material. One example is the N-V-centre defect, which comprises of a nitrogen atom having been incorporated in the diamond lattice, see Figure 5. Other defects include doping with boron or nickel [3]. These confer certain electronic and optical properties to the nanodiamond particles.

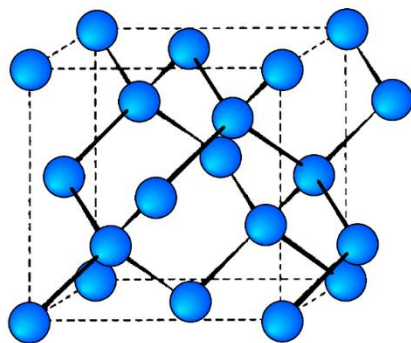


**Figure 4:** Cubic lattice of diamond. [1]

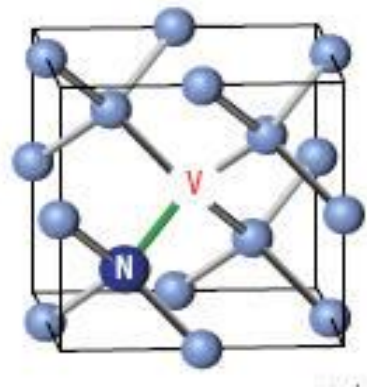
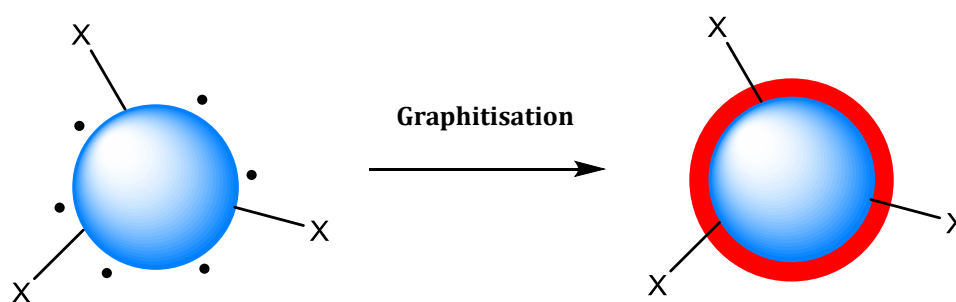


**Figure 5:** N-V centre defect. [4]

### 1.1.3.2. Surface Structure

The surface structure of any nanomaterial can exert considerable influence upon its physical and chemical properties as the ratio of surface atoms per mass increases the smaller a particle gets. In the range of diameters commonly seen for particles generated via detonation for example, i.e. ~ 5 nm, approximately 30 % of the atoms are situated on the surface [2].

The carbon atoms comprising the surface are coordinatively unsaturated and possess at least one unsaturated bonding site. These so called 'dangling bonds' are rather energetically unfavourable and in turn several processes exist to ensure complete saturation of these positions [3]. They include reactions with external partners as well as the reconstruction of the surface leading to the formation of more or less conjugated  $\pi$ -bonds. In the case of  $\pi$ -bond formation, a partial graphitisation of the particle surface occurs, see Scheme 2.



**Scheme 2:** Graphitisation of nanodiamond surface via dangling bonds.

Besides partial graphitisation, a variety of functional groups can also exist on the nanodiamond surface. The standard elemental composition of detonation nanodiamond points towards a dense covering of oxygen containing groups, see Table 1.

Material	C	H	N	O
Nanodiamond	80 - 90	0.5 - 1.5	2 - 3	0.5 - 12

**Table 1:** Elemental composition (%) of nanodiamond [3].

It is worth noting however, that the elemental composition is not always a clear indicator of the nanodiamond surface functionality, as it can also be influenced by impurities detected in the sample. These include metals from the reactor wall and considerable amounts of water. The latter is easily adsorbed on the surface of the nanodiamond, thus often accounts for the majority of the

oxygen detected in the sample. It can be removed by heating *in vacuo*, yet a partial graphitisation is accepted in doing so, if too high a temperature is used. Metallic impurities can be removed by treatment with strong mineral acids such as  $H_2SO_4$ , which often results in oxidation of the nanodiamond surface, with the purified samples exhibiting pronounced signals for various carbonyl functions in their IR spectra [6].

It is also worth noting that for those samples obtained by 'wet' detonation synthesis, i.e. where water was used as the coolant, a dense covering of hydroxyl groups can also be obtained. Other functional groups assigned to the surface include the carboxylic acid, lactone, amide and ester groups. Thus, it becomes clear that the nanodiamond surface is comprised of a variety of oxygen containing groups, as opposed to some form of homogeneous covering, see Figure 6.

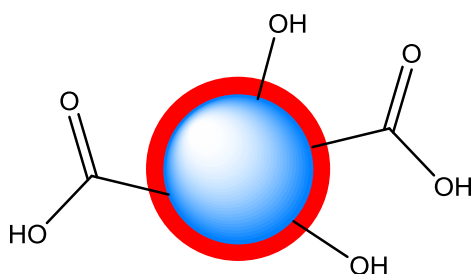


**Figure 6:** Typical surface coverage of detonation nanodiamond.

#### 1.1.4. Properties of Nanodiamond

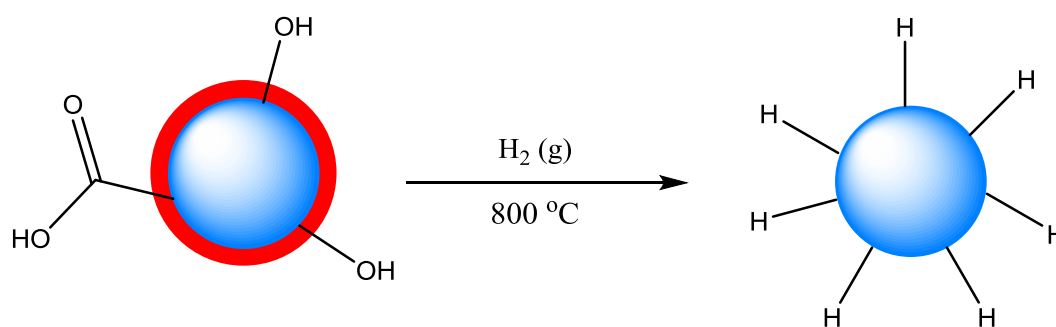
##### 1.1.4.1. Chemical Properties

In comparison to bulk diamond, nanodiamond is significantly more reactive, a property that arises from the enlarged surface area and high number of defects associated with the nanomaterial. Both effects increase the number of potential sites of attack for a reagent, thus enabling the surface of the nanodiamond to undergo chemical modification [7].

As previously stated the nanodiamond surface is comprised of a number of highly reactive 'dangling bonds' with each atom on the surface possessing at least one unsaturated bonding site. These are particularly high in energy as saturation of the free vacancies typically occurs via  $\pi$ -bond formation. The resulting  $sp^2$  hybridised domains exist as isolated double bonds or condensed aromatic type structures. Therefore a possible strategy for the functionalisation of the nanodiamond surface could involve using a class of reactions ubiquitous to olefins or aromatics, i.e. the Diels-Alder reaction [1]. The problem with this strategy, however, is that the bonding between the diamond core and graphite outer layer would be so weak (van der Waals forces only) that the functionality would be attached to a kind of shell, as opposed to the actual diamond core.

As a result, the instability of the functionalised nanodiamond particles could become problematic, particularly if used in mechanically straining applications. Instead, a more effective approach could involve direct covalent linkage to the nanodiamond surface after the removal of any graphitic domains.

As well as the graphitic domains, detonation nanodiamonds also possess a primary surface functionalization comprising of a multitude of oxygen containing groups, many of which can undergo chemical reactions directly to form secondary products. A homogenisation of the primary functionalities is often required however, to ensure a reproducible quality of the secondary products obtained. Surface homogenisation can be achieved using a range of methods; with one of the most prevalent involving some form of thermal treatment in air, with temperatures exceeding 800 °C [1]. This results in the complete removal of any surface functionality and a partial graphitisation of the outermost shell. Other methods employed require the use of a chemical reagent, often some form of oxidant or reductant. For these techniques, surface homogenisation is achieved by creating a uniform coverage of only one type of functional group on the nanodiamond surface. Reductive homogenisation is conventionally achieved via thermal treatment with hydrogen gas in a tube reactor [8], see Scheme 3. The new C-H bonds can then undergo photolysis for subsequent functionalisation. Methods to attain homogeneous oxidation will be discussed later in section 1.1.5.1. .



**Scheme 3:** Hydrogenation of nanodiamond surface.

### 1.1.4.2. Electronic Properties

Nanodiamonds possess an array of interesting electronic properties and as such demonstrate great potential for a number of electrical applications. These properties are all quite complicated, dependant on a range of different variables, i.e. particle size, surface functionality, etc. The amount of  $sp^2$  hybridised carbon present in a nanodiamond sample for example, can have a drastic effect on its electrical conductivity. More specifically, Kovalenko *et al* [9] reported a twelve order of magnitude increase in the electrical conductivity of a nanodiamond sample, when the amount of  $sp^2$  hybridised carbon present was increased from 1 to 50 %. This increase in electrical conductivity was due to a pronounced p type conductivity of the graphitic domains, with a concentration of holes reaching a maximum of  $10^{13} \text{ cm}^{-2}$  [9].

Particle size also influences the nanodiamond's electronic properties, as smaller particles lead to a larger portion of the carbon atoms being situated on the surface, thus increasing the amount of  $sp^2$  hybridised carbon present in the sample. A consequence of this is observation of an additional band structure for nanodiamond when compared to the bulk material, see Figure 7. Despite this, the electronic properties of the diamond core strongly resemble those of the bulk material, with the width of the band gap almost identical, ca. 5.5 eV, for both materials [3].

The presence of impurities in the nanodiamond core can also drastically alter electronic properties, with defects of this kind giving rise to additional energy levels within the band gap that may or may not be occupied by electrons. For example, the conductivity of nanodiamond is further increased by nitrogen lattice defects and by surface doping.

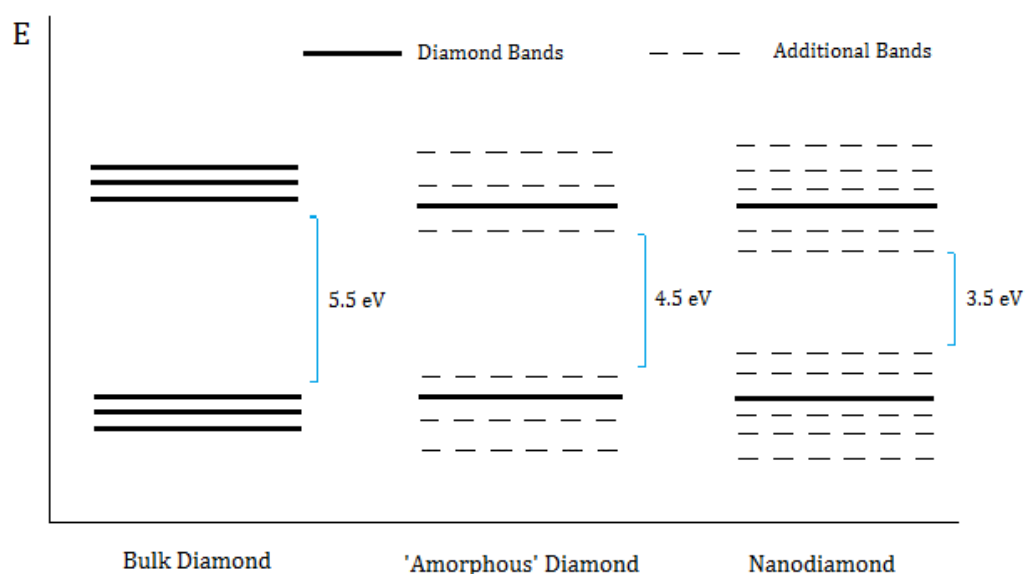


**Figure 7:** Comparison of surface band structures of bulk diamond and nanodiamond.

One of the most exciting electronic applications for nanodiamond is in the field of electrorheology [10]. Electrorheological fluids are suspensions of extremely fine non-conducting particles in electrically insulating fluids. In response to an electric field, the viscosity of these fluids can change reversibly by up to five orders of magnitude. For example, a typical electrorheological fluid can change from the consistency of a liquid to that of a gel, and back, in a couple of milliseconds. This effect is known as the Winslow effect [10], and may be of great use in the development of flexible electronics, with fluid incorporated in elements such as rollable screens. The viscosity changing qualities of the electrorheological fluid will allow the flexible elements to become solid when in use and flexible to roll for storage, see Figure 8.



**Figure 8:** Flexible electronics. [10]

#### 1.1.4.3. Mechanical Properties

Diamond's distinct mechanical properties are dominated by its three-dimensional orthotropic lattice structure, within which each carbon atom forms a minimum of four C-C covalent bonds. Covalent bonds are an essential prerequisite for the hardness of any material, thus with each carbon forming a minimum of four bonds, of the order of  $350 \text{ kJ mol}^{-1}$  [11], it is of little surprise to hear that diamond is the hardest natural material on earth. Generally, the mechanical properties of macroscopic diamond are also largely true for the nanoscale material as they possess the same crystal structure. This is particularly true for the bulk modulus and shearing strength which are virtually unaffected by the particle size [12]. The hardness of the nanodiamond is slightly reduced in comparison to the bulk however, as the nanoscale diamond particles possess  $sp^2$  hybridised domains on the surface. Depending on the dimensions of the nanodiamond particles, they can be used either as abrasives or lubricants. Classically, particles with a diameter above 100 nm exhibit abrasive effects, whilst those with a diameter below 100 nm are almost frictionless [3].

#### 1.1.4.4. Biological Properties

Nanodiamond is an attractive material for numerous biomedical applications, principally due to its low toxicity and chemical inactivity [1]. Bondar *et al* [13], have demonstrated that a number

of biological moieties could be fixed to the nanodiamond surface, either covalently or non-covalently, whilst retaining their functionality. Most publications to date tend to describe non-covalent adsorption of proteins, antibodies, pharmaceuticals onto the nanodiamond surface [1], see Figures 9 and 10. There is also real potential for nanodiamond as a viable drug delivery vehicle.

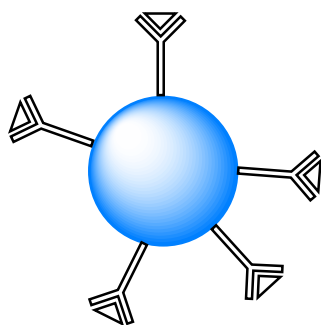


**Figure 9:** Antibodies bound to the nanodiamond surface.

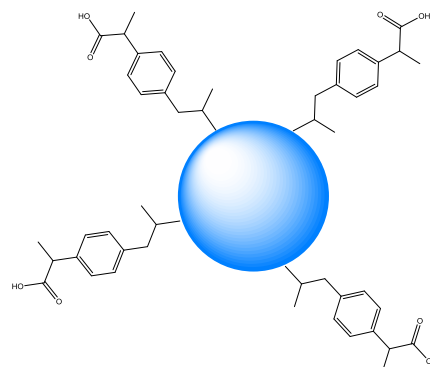


**Figure 10:** Pharmaceutical bound to the nanodiamond surface.

### 1.1.5. Nanodiamond Surface Functionalisation

The possibilities for a versatile surface functionalisation of nanodiamond are endless. Various methods for the production of functional nanodiamond particles have been reported and the availability of surface groups for all kinds of subsequent grafting reactions have significantly improved over the last ten years [1]. It is now the case where almost any organic functional group could, in theory, be incorporated into the nanodiamond surface. Oxygen containing moieties are especially easy to obtain, owing to the oxidised nature of the nanodiamond particles following detonation synthesis. This is particularly useful, as oxygen containing groups are often quite reactive, thus can be used as versatile anchor groups for the immobilisation of larger moieties.

In one case, Ho *et al* [14] utilised a homogenous covering of hydroxyl groups to immobilise bovine insulin onto the nanodiamond surface. Other interesting groups that have been immobilised onto nanodiamond include cytochrome C [15], lysozyme [16] and apoobelin [17]. Notably all of these molecules retained their functionality upon immobilisation, thus the use of nanodiamond as a vehicle for drug delivery could be entirely feasible, seeing that nanodiamond is biocompatible. By grafting drug molecules on the nanodiamond surface, these conjugates could be used to solubilise lipophilic compounds that may otherwise be difficult to deliver to the body, i.e. they do not obey Lipinski's Rules. Again, Ho and co-workers [18] have demonstrated this by immobilising doxorubicin, an anti-cancer agent, onto nanodiamond for sequential release.

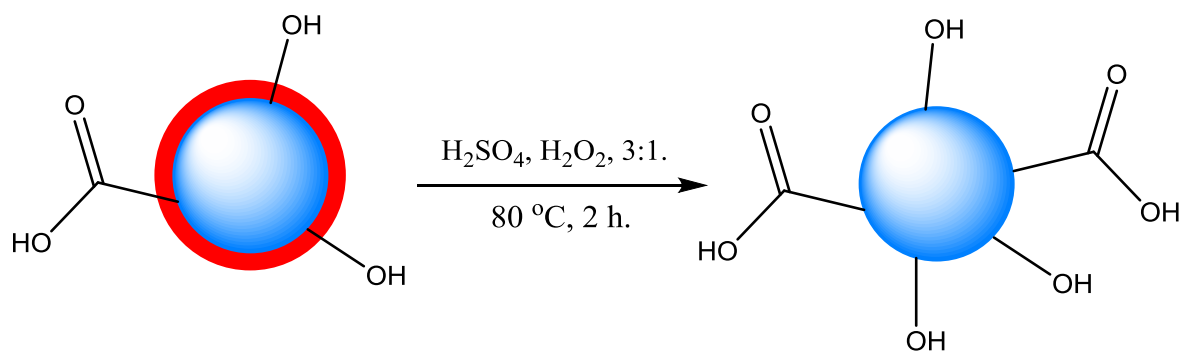
### 1.1.5.1. Oxidation

As mentioned previously, nanodiamonds produced by detonation synthesis always exhibit some form of primary surface functionalisation; often this consists of a multitude of different oxygen containing groups as well as a number of amorphous graphitic domains. To ensure a reproducible quality of any secondary products, a homogenisation of the primary functionalities is required. Several strategies could be employed to achieve this, with those involving some form of oxidation often being the most effective; these are the oxidative purification methods.

There are two main methods for oxidative purification; the first requires the use of a harsh oxidant in aqueous solution [19], and the second calls for thermal treatment in air [20]. Both methods are accompanied by inevitable material loss and size reduction of the diamond core, with the evolution of CO<sub>2</sub> and CO as oxidation products.

The first method is carried out using a mixture of strongly oxidising mineral acids. A successful mixture consists of equal amounts of concentrated sulphuric, nitric and perchloric acid. The use of 'piranha solution', a 3:1 mixture of concentrated sulphuric acid and hydrogen peroxide is also standard [21]. Purification is based upon the principal that the reactivity of graphite towards oxidation is far higher than that of diamond. Hence, the disordered sp<sup>2</sup> hybridised carbon is lost as CO<sub>2</sub> gas, whilst the diamond is conserved. The diamond is not fully inert to oxidation however, as it becomes partially oxidised instead with a dense covering of oxygen containing groups having been generated on the surface, see Scheme 4. Removal of the graphitic domains previously bound to the nanodiamond surface can be detected using X-ray powder diffraction. It is also worth noting that acid treatment can result in the effective removal of metallic impurities originating from the reactor.

The second oxidative technique involves thermal oxidation of the nanodiamond in air. First reported by Gogotsi *et al* [20], it was found that temperature is a key component in controlling the selective oxidation of amorphous carbon. Their results suggested that a minimum temperature of 400 °C was required for the onset of oxidation of the sp<sup>2</sup> hybridised carbon, and that any temperature above 450 °C resulted in diamond loss [20].



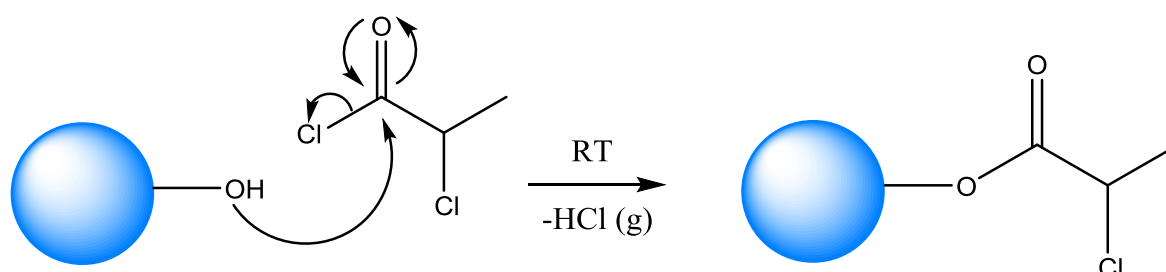
**Scheme 4:** Oxidation of the nanodiamond surface.

### 1.1.5.2. Chlorination

Chlorination constitutes one of the most valuable methods of nanodiamond surface functionalisation, with chlorinated nanodiamond a key intermediate in the pathway to further functionalisation. One of the most dependable methods for introducing chlorine onto the nanodiamond surface is the gas phase reaction of  $H_2$  and  $Cl_2$ . The reaction is performed in a tubular reactor heated to  $400\text{ }^\circ\text{C}$ , and a mixture of elemental chlorine and hydrogen gas is passed over the sample. First devised by Khabasheku *et al.* in 1997 [22], it has since been used as a key intermediate reaction for a countless number of functionalisation reactions.

Chlorination could also be conducted photochemically using a mercury vapour lamp [7]. This method is particularly effective as both  $sp^2$  hybridised carbon atoms and pre-existing functional groups are subject to attack from the chlorine free radicals. As such this technique can effectively restore the  $sp^3$  hybridised state across the entire nanodiamond surface, as the graphitic regions are lost and homogenisation of the bonding situation occurs. There is however, a definite issue concerning this method of direct chlorination, i.e. the instability of the C-Cl bond. These bonds are susceptible to attack from any form of nucleophilic reagent and can even react with atmospheric water. The main source of reactivity is the ability of the chlorine to act as a good leaving group, and the relative stability of the tertiary carbocations left behind. Hence, effective storage in the lab is rarely achieved without loss of the chlorine surface groups [22].

In a bid to establish a more stable covering of chlorine on the surface, a more effective approach might involve grafting chlorine to the surface as the terminal moiety of a short, inert linker molecule. An example of this method was reported by Zhang *et al* [23], where the hydroxyl groups on the nanodiamond surface were modified with the initiator, 2-chloropropionyl chloride. In this case, the ND-Cl was stable enough for storage in the lab without a compromise to the surface functionality. Hence, the ND-Cl could then be used in a series of other reactions, i.e. ATRP.



**Scheme 5:** Chlorination of the nanodiamond surface using the initiator 2-chloropropionyl chloride.

### 1.1.6. Nanodiamond Composites

Nanodiamond composite design exemplifies the cutting edge of science, constituting an entirely new field of research. Having only emerged within the last three years, this field has great scope for further exploration, with a particular emphasis on the potential applications of the new composites. Nanodiamond is well suited to composite design, as it possesses a unique array of properties that complement many polymer matrices [24]. These include its unique hardness, good biocompatibility and ease of surface functionalisation. In terms of synthesis, the nanodiamond composites can be prepared by incorporating the nanodiamond into the polymer matrix either covalently or non-covalently [24].

#### 1.1.6.1. Non-Covalent Nanodiamond Composites

Numerous examples of non-covalently bound nanodiamond composites have been reported in the literature [3], although little is understood of the interaction between the nanodiamond and the polymer matrix. It is possible that this is due to the variable nature of the nanodiamond surface, featuring both  $sp^2$  hybridised domains, and a variety of polar and non-polar functional groups.

Non-covalent incorporation of the nanodiamond into the polymer matrix is achieved by simple admixing during polymerisation. Some examples of the polymers that have been incorporated with nanodiamond in this way include the polysiloxanes, fluoroelastomers and epoxy resins [3]. Remarkably, all of the examples above exhibited some form of mechanical enhancement upon nanodiamond incorporation, see Table 2. In all cases, the modulus of elasticity, the tensile strength and the maximal elongation of the materials increased. This was quite a result, especially when one considers the nanodiamond loadings were as low as 0.1 – 0.5 wt % [3].

<b>Polymer</b>	<b>Modulus of Elasticity/ MPa</b>	<b>Tensile Strength/ MPa</b>	<b>Maximum Elongation (%)</b>
Polysiloxane	19	52	730
Polysiloxane Nanodiamond Composite	53	154	1970
Fluoro Elastomer	8.5	15.7	280
Fluoro Elastomer Nanodiamond Composite	92	173	480

**Table 2:** The effect of non-covalent incorporation of nanodiamond on various polymers.

#### 4.1.6.2. Covalent Nanodiamond Composites

The covalent incorporation of nanodiamond into the polymer matrix has been studied to a far lesser extent, with only two types of polymer, polyurethanes and epoxy resins, having undergone successful covalent nanodiamond incorporation [24]. Both materials have displayed a marked improvement in mechanical properties, in much the same way as the non-covalent nanodiamond polymer composites. This would have been due to the capacity of the nanodiamonds to act as sites for cross-linking of the polymer chains in the polymer matrix. Compared to non-covalent incorporation, direct covalent incorporation is also thought to result in a more homogenous distribution of nanodiamond within the polymer matrix. In turn the uptake of mechanical load by the covalently incorporated nanodiamond composites is thought to be far more efficient [3].

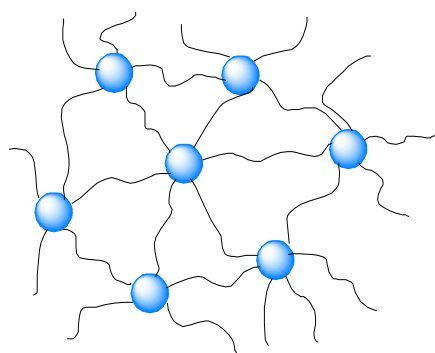


**Figure 11:** Covalently incorporated nanodiamond composite.

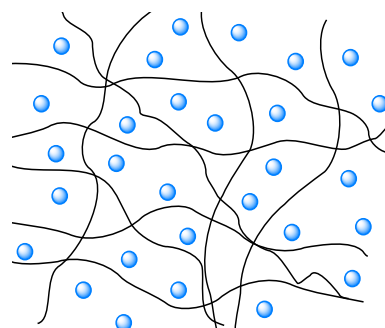


**Figure 12:** Non-covalently incorporated nanodiamond composite.

## 1.2. Hydrogels

Over the last ten years, the extent of research relating to self-assembled hydrogels has expanded rapidly as we seek to explore their full range of potential applications. The term hydrogel refers to a three-dimensional network of cross-linked polymer chains that can absorb and retain water well. Hydrogels can be classified according to their origin or the type of cross-linking present within their three-dimensional polymer matrix [25].

### 1.2.1. Hydrogel Classification

Hydrogels can be prepared using either natural or synthetic starting materials, natural hydrogels are generally derived from proteins or polysaccharides, as they have a tendency to form self-assembled three-dimensional structures when dissolved in water [26]. This is facilitated by the high number of intermolecular interactions that exist between the discrete polymer chains. An example is the extracellular matrix (ECM) that forms the main component of human tissue [25]. Essentially, the ECM provides mechanical and structural support to the cells, but also forms the

main component of our connective tissue, see Figures 14 and 15. The interstitial matrix is comprised of a polysaccharide gel dispersed with fibrous protein, which in combination act as a compressive buffer against the stress placed on the ECM. Other examples of naturally derived hydrogels include gelatine, collagen and hyaluronic acid. Synthetic hydrogels on the other hand, are derived from man-made constituents such as poly (vinyl) alcohol or acrylamide [26].

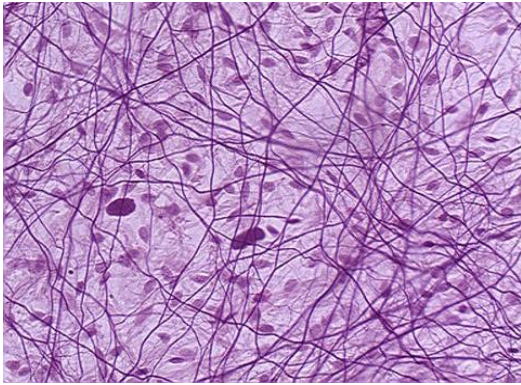


**Figure 14:** ECM Hydrogel. [25]

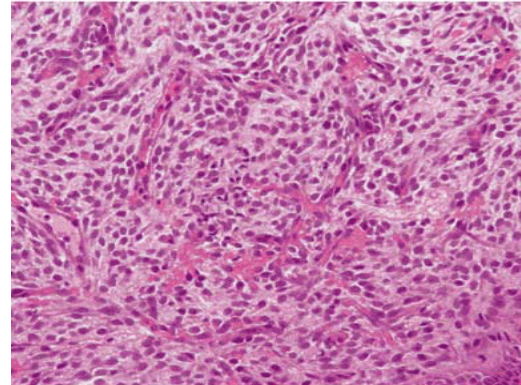


**Figure 15:** ECM Hydrogel. [25]

As mentioned previously, hydrogels can also be classified in accordance to the type of cross-linking found within the polymer matrix. There are two classes, the 'permanent chemical' hydrogels and the 'reversible physical' ones [26]. The permanent gels possess a covalently cross-linked polymer matrix and attain an equilibrium swelling state depending on the polymer-water interaction parameter and the crosslink density. These hydrogels are often brittle in nature and shatter upon the application of high pressure. Conversely, the reversible gels possess a polymer matrix held together by molecular entanglement and secondary forces including ionic, hydrogen bonding and hydrophobic interactions. These interactions are considerably weaker than the covalent bonds of the permanent gels; hence the reversible gels are 'self-correcting'. This means that they can adjust to external pressure, thus resolving any issue of 'brittleness'.

### 1.2.2. Hydrogel Properties

The water holding capacity of a hydrogel is one of its most distinguishable features. This is a description of how much water a gel can absorb when placed in aqueous solution [26]. Uptake of the water begins with the initial hydration of the hydrophilic groups at the surface of the gel. The gel then absorbs additional water due to the osmotic driving force of the network chains towards infinite dilution. An equilibrium level of swelling is then reached, where no more water can be absorbed. The equilibrium level of swelling is determined by the degree of cross-linking in the polymer matrix, i.e. physical or chemical, and results in a net elastic network retraction force [26].

As well as the ability to uptake water, hydrogels also possess other interesting properties. Many are biodegradable, making them suitable for a range of biomedical uses, i.e. in drug delivery, tissue engineering and wound healing [25]. Biodegradable hydrogels contain labile bonds present either in the polymer backbone or in the cross-links used to synthesise the gel. These bonds can be broken under physiological conditions either chemically or enzymatically, hence degradation of the gel occurs naturally. Uses in drug delivery and wound healing also require the hydrogel to be biocompatible. The biocompatibility of a material describes how well it can come into contact with a biological system without triggering an immunological response or causing any long-term adverse biological effects [25]. Hydrogels possess a good degree of biocompatibility because the interfacial free energy between the surface of the hydrogels and the cellular components of the body are low, i.e. proteins and cells have a low tendency to adhere to the surfaces [25].

Hydrogels also possess a variable elastic behaviour. This is determined by the amount of water retained in the polymer matrix and the extent of polymer cross-linking within the material. The variable elastic behaviour of a hydrogel could have many uses, e.g. to create a material possessing the same degree of flexibility as natural tissue [25].

In literature some hydrogels have even been reported to demonstrate stimuli-responsive behaviour [27]. Classically, this involves a change in the volume of the hydrogel in response to a given stimulus, i.e. a change in pH, temperature, and light intensity. One class of stimuli-responsive hydrogels that have been studied extensively are the thermogels, these are temperature responsive. Some examples of the temperature responsive hydrogels include poly (vinyl methyl ester) and poly (N-isopropyl acrylamide) gels [27].

### 1.2.3. Mechanisms of Hydrogel Formation

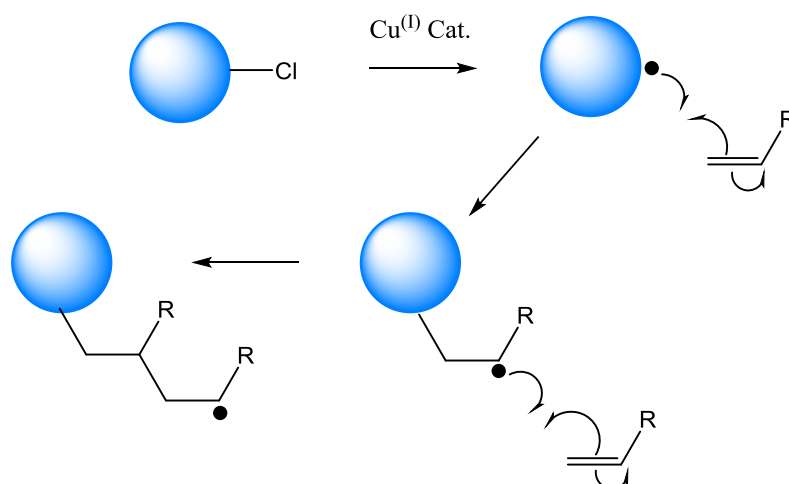
The mechanism that facilitates hydrogel formation is one that is well defined in the literature; conventionally referred to as gelation [26]. The first step involves the formation of a 'sol', a mixture of polydisperse soluble branched polymers. The 'sol' is produced by the initial cross-linking of free polymer chains in solution, leading to the formation of progressively larger branched polymer chains. These remain soluble in solution however, and it is only after considerable further cross-linking that the 'infinite polymer' or gel is formed. This transition from a system of finite branched polymers to infinite molecules is known as the 'sol-gel' transition. The critical point where the gel first appears is referred to as the 'gel point'.

Gelation can take place either by physical or chemical cross-linking as mentioned previously. Chemical gelation involves the formation of covalent bonds between the polymer chains and always results in a 'strong' gel. The three main chemical gelation processes include condensation, vulcanisation and addition polymerisation. In this experiment however, the focus will only be on the latter or more specifically a type of addition polymerisation known as atom transfer radical polymerisation, ATRP.

### 1.2.4. Atom Transfer Radical Polymerisation

First developed by Matyjaszewski *et al* in 1995 [28], this method of polymerisation offers an efficient route for synthesising polymers with well-defined molecular weights and polydispersity. It is essentially a type of 'living' polymerisation, where the ability of a growing polymer chain to terminate has been removed, meaning that the polymer chains grow at a constant rate and their molecular weights remain the same [29]. In older text books, ATRP may also be classified as a type of addition polymerisation, since the empirical formula of the polymer produced is simply the sum of the required number of monomers.

In terms of mechanism, polymerisation proceeds via a radical chain growth process, as outlined in Scheme 6.



**Scheme 6:** Atom transfer radical polymerisation, ATRP.

The first step, the initiation step, involves the abstraction of a halogen atom from the initiator molecule to generate a reactive free radical species [30]. Abstraction of the halogen is facilitated by a transition metal complex, typically  $[\text{Cu(I)}(\text{bpy})_2\text{Cl}]$ , which itself undergoes a one electron oxidation. A copper catalyst is classically used because both the Cu(I) and Cu(II) oxidation states are readily available and copper has a high affinity for halogens, such as chlorine. The reactive radical species can then attack the carbon-carbon double bond of the given monomer, generating a free radical intermediate. This process is described by the rate constant,  $k_i$ . Polymer chain growth then proceeds via the addition of sequential monomer units. The rate of chain growth is described by the rate constant,  $k_p$ . Growth of the polymer chains stops when the monomer starting material has been used up, resulting in the uniform growth of all chains and a low polydispersity. Chain termination is limited, as no more than 5 % of the total growing polymer chains terminate during the initial, non-stationary stage of polymerisation [30].

Various monomers have been successfully polymerised via ATRP; methacrylates, methacryl amides, dienes, etc. all of which result in the formation of a stable hydrogel in the presence of a short, inert cross-linker such as diethylene glycol dimethacrylate [30]. ATRP is a particularly useful method for synthesising hydrogels, as it always produces monodisperse, high molecular weight polymer chains, thus making the gel as homogenous as possible [31].

### **1.2.5. Hydrogel Applications**

Hydrogels show great promise for a wide array of potential applications, with uses as far afield as tissue engineering, electronics and mechanochromic sensing, all of which are being developed to tackle real and very urgent global problems [25]. The shortage of organs for transplant for example, could be addressed using hydrogels, with scientists proposing tissue engineering as the answer to the problem. The main principle of tissue engineering is founded upon the idea that an entire organ could be grown artificially in the laboratory. It is particularly beneficial, as the need for an organ donor would be removed, and the organs themselves could be modelled using the patient's DNA, thus eradicating any issues of transplant rejection. One approach that seems particularly promising is referred to as 'organ printing' [32]. This involves 'printing' a three-dimensional cell scaffold of an organ using a thermal responsive hydrogel 'ink'. The printed structures can then be heated to form permanent gel scaffolds which can later be embedded with stem cells to initiate tissue generation [33]. Thus, it is easy to see how the fabrication of an entire organ could soon be made possible.

Another interesting hydrogel application concerns the development of photonic sensory films. First reported by Thomas *et al* [34], these photonic hydrogel films have the capacity to reflect a

wide range of wavelengths in response to a variety of stimuli. As such these gels could have various uses as colorimetric chemical sensors, i.e. in therapeutic imaging.



**Figure 15:** Hydrogel scaffold ear. [33]

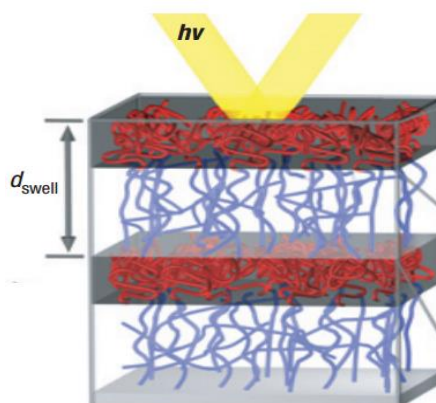


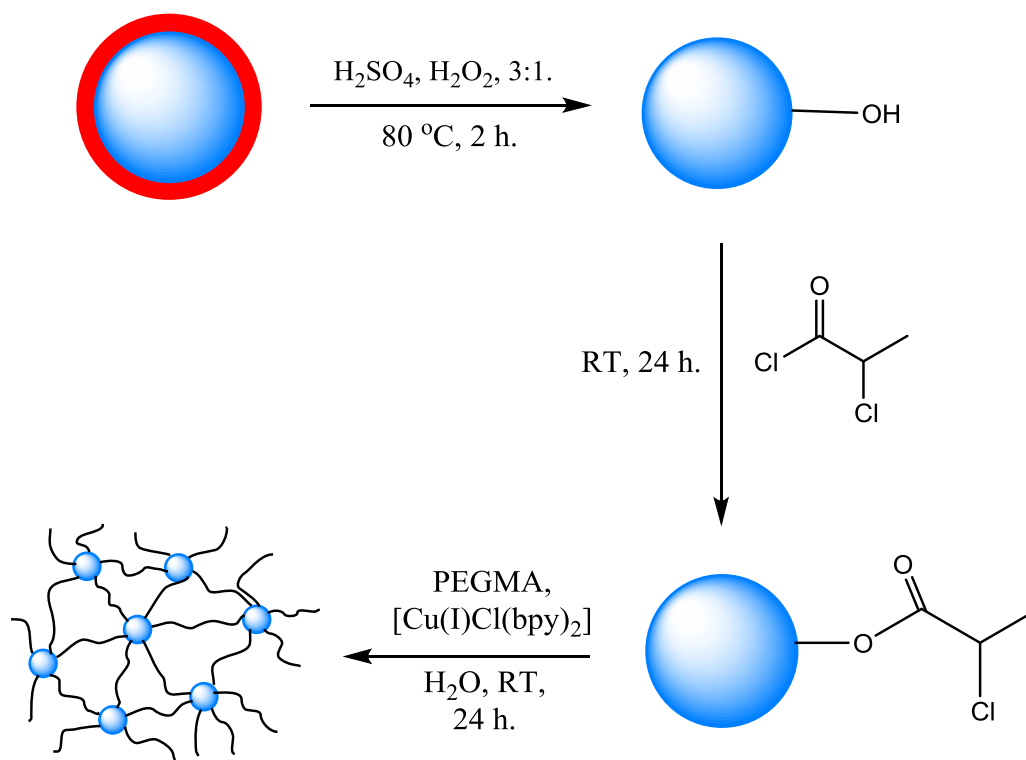
**Figure 16:** Photon sensory film. [34]

### 1.3. Nanodiamond Hydrogels

Upon recognising the potential in the field of nanodiamond composite research, it was decided that the aim of the project would be to devise a method for synthesising a new class of nanodiamond composite, one in which an array of functionalised nanodiamond particles would be covalently incorporated within a three-dimensional polymer matrix. This would constitute the so-called 'nanodiamond hydrogel', and to our knowledge would be the first of its kind. If synthesis was to be successful, it is likely that the composite would possess a number of interesting properties, many of which would be suitable for a multitude of potential applications, see section 1.3.2.

### 1.3.1. Strategy for Synthesis

Synthesis of the covalently incorporated nanodiamond hydrogels was pursued by means of atom transfer radical polymerisation, otherwise known as ATRP, see section 1.2.4. An overview of the steps comprising the synthesis is outlined in Scheme 7.



**Scheme 7:** Strategy for synthesis of covalently incorporated nanodiamond hydrogel.

The first stage of the synthesis was a homogenisation of the surface functionality of the nanodiamond starting material; in this case to maximise the number of hydroxyl groups on the surface of the nanodiamond. An effective method of oxidation requires the use of ‘piranha solution’, a 3:1 mixture of concentrated  $\text{H}_2\text{SO}_4$  and  $\text{H}_2\text{O}_2$  [21]. Piranha solution is of particular use as unlike other oxidants, it also eliminates any traces of graphite on the nanodiamond surface which would otherwise hinder the reactivity of the hydroxyl groups present, and comprise the mechanical strength of the end product. The second stage of synthesis required reacting the hydroxyl groups on the surface of the nanodiamond with an initiator, i.e. 2-chloropropionyl chloride [23]. The nanodiamond was then ‘initiated’ and thus able to facilitate ATRP of the selected monomer, in the absence or presence of a suitable cross-linker [35]. The mechanical properties of the nanodiamond composites were then determined via a series of rheological tests.

### 1.3.2 Nanodiamond Hydrogel Applications

As described previously, if synthesis is successful, the nanodiamond hydrogels will represent an entirely new class of composite material, and as such may possess a number of interesting properties, many of which will be suitable for a multitude of potential applications. Some of these include uses in mechanical reinforcement, protective UV films and the enhancement of capacitance.

Within the last three years, the expanse of research concerning the use of hydrogels in soft electronics has seen unprecedented growth [25]. Much of this work has been focused upon the development of hydrogel supercapacitors. These are devices that can be used to complement batteries in terms of energy storage, providing quick bursts of power when required, which have great potential in the automotive industry, see Figure 17. The hydrogels in question are comprised of electrochemically active polymers such as poly (aniline) and can be used to replace the standard carbon electrodes found in conventional supercapacitors [36]. The new hydrogel-based materials are particularly attractive as they possess a capacitance approximately three times greater than that of the conventional carbon analogues at a fraction of the cost [36]. Hydrogel based capacitors are particularly cost-effective as the electrolyte used is water-based, thus significantly cheaper than the organic alternatives used for carbon supercapacitors. In addition, the fabrication of the hydrogel-based materials is feasible both on the large and small scale, encompassing uses in mass energy storage and microelectronics [36].

There is however one major problem associated with hydrogel-based capacitors; this is their lack of long-term stability caused by significant changes in volume during operation [36]. Essentially, the hydrogel electrode components of the supercapacitors swell and contract rapidly upon charge and discharge. Over a sustained period of time, i.e. after 10,000 cycles, this causes the gels to disintegrate resulting in decreased electrical conductivity of the electrodes, leaving the system redundant [9]. This is a significant problem and is currently hindering the use of hydrogel-based capacitors in any form of industrial application.

However, it is thought that the covalent incorporation of nanodiamond into the hydrogel matrix could offer a potential solution to this problem. The idea is that the incompressible nanodiamond additive embedded in the hydrogel could serve as a toughening agent, minimising the volume changes of the hydrogel electrode, thus preventing disintegration of the hydrogel components, recent work by Kovalenko *et al*, is very promising [9].

To the same effect, it is also thought that nanodiamonds could be interfaced with hydrogel polymer matrices to confer mechanical reinforcement. Covalent incorporation is believed to be

the best method of introducing the nanodiamond into the polymer matrix, as other traditional polymer processing techniques such as casting and extrusion have yielded poor dispersions due to agglomeration of the nanodiamond particles within the matrix [3]. Nanodiamond hydrogel composites could be used for a variety of biomedical applications including cell growth scaffolding and wound dressing. Fluorescent nanodiamond hydrogels also have potential uses in medical diagnostics and photovoltaics.

Covalently incorporated nanodiamond hydrogels could be used to develop thin UV protective films also, see Figure 18. These films could have a variety of applications, including coating windows or preventing the degradation of UV sensitive materials [34]. Nanodiamond hydrogel composites are suited well to these applications as nanodiamond absorbs selectively in the UV range only, i.e. it remains transparent in the visible region.

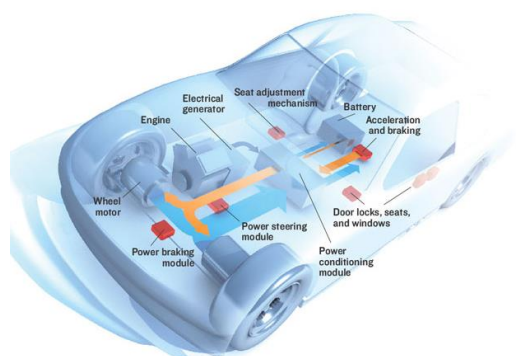


**Figure 17:** Car with supercapacitor battery, orange arrows show how supercapacitor discharges to power acceleration, and blue arrows highlight energy flowing back during breaking. [36]

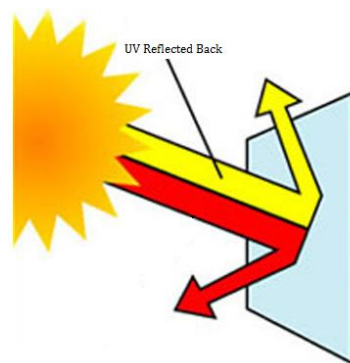


**Figure 18:** UV protective films. [34]

## 1.4. Characterisation

Throughout the project, various methods of characterisation were used to examine the nature of the products made during each step of the nanodiamond hydrogel synthesis. In the following section, there is a brief outline of each of the techniques used.

### 1.4.1. Fourier Transform Infrared Spectroscopy

In order to ascertain whether or not successful functionalisation of the nanodiamond surface had taken place, nanodiamond samples were characterised by means of Fourier transform infrared spectroscopy, FTIR. This technique works on the principle that each of the covalent bonds found within a molecule, or in this case on the surface of the nanodiamond, vibrate at a slightly different frequency as described by Hooke's Law, thus when exposed to a source of infrared radiation each

of the bonds absorbs at specific wavelength [37]. As a result, every molecule possesses a unique infrared absorbance spectrum, one in which the absorption frequencies correspond to the specific bonds found within the molecule. Notably, those bonds that display the greatest change in dipole moment during vibration, tend to correspond to the peaks of highest intensity, i.e. the C=O and C-O bonds. For this study, the peaks of greatest interest corresponded to the O-H and C-Cl stretches, as these were indicative of successful surface functionalisation.

#### **1.4.2. Raman Spectroscopy**

Raman spectroscopy was used to confirm successful incorporation of the nanodiamond into the polymer matrix of the hydrogel. This was possible as the Raman spectrum for nanodiamond is unique, and thus identified with ease. For bulk diamond, there is a sharp signal at  $1322\text{ cm}^{-1}$  corresponding to a triply degenerate optical  $\Gamma$  phonon mode [3]. For nanoscale diamond however, this band is shifted to  $1332\text{ cm}^{-1}$ , demonstrating a size effect [3]. Raman spectroscopy is similar in principle to IR, as it is also based upon the absorption of light by a sample. To be more specific, it works by determining how the energy of a monochromatic source of light can be shifted upon interaction with the molecular vibrations, phonons or other excitations of a chemical sample.

#### **1.4.3. X-Ray Powder Diffraction**

X-ray powder diffraction is a tool used to determine the position of atoms in a crystalline structure. In this experiment, it was used to probe the structure of nanodiamonds before and after oxidative treatment with piranha solution. This was to ascertain whether or not the oxidant was capable of removing any traces of graphite on the nanodiamond surface. If successful, one would expect the diffraction pattern for the oxidised sample to exhibit those peaks characteristic of  $sp^3$  hybridised diamond only, i.e. at  $2\theta = 43.9, 62.5, 75.3$  and  $91.5^\circ$  [38]. X-ray powder diffraction is founded upon the principal that X-rays possess a wavelength comparable to the atomic spacings of a typical crystal structure, thus when a beam of X-rays is fired at a crystalline sample, diffraction will occur. This produces a diffraction pattern unique to the crystal structure of the given sample.

#### **1.4.4. Scanning Electron Microscopy**

In order to assess the size and morphology of the nanodiamonds after each functionalisation step, the particles were imaged using scanning electron microscopy, SEM, a technique that produces an image by scanning the surface of the sample with a focused beam of high energy electrons. The electrons are then reflected elastically from the surface of the sample and detected to construct a two dimensional picture of the surface. Resolutions of up to 1 nm can be achieved [39].

#### **1.4.5. Transmission Electron Microscopy**

This technique was used alongside SEM to assess the size and morphology of the nanodiamonds before and after functionalisation. Transmission electron microscopy, TEM, works by firing a beam of electrons through an ultra-thin sample and focusing the beam onto an imaging device, i.e. a fluorescent phosphor screen [40]. The resolutions achieved using TEM are often higher than those for SEM.

#### **1.4.6. Dynamic Light Scattering**

A quantitative analysis of the size of the nanodiamond particles was also vital, this was achieved using dynamic light scattering, DLS. Also known as photon correlation spectroscopy, this technique measures the size distribution of the particles in a colloidal suspension by recording the degree of scattering that occurs when a source of monochromatic light is passed through a sample [41]. Parameters required to calculate the size distribution of the suspension include the refractive index of the solvent and the viscosity of the sample.

#### **1.4.7. Rheological Tests**

A series of rheological tests were carried out to quantify the mechanical properties of the nanodiamond hydrogels. These required the use of a rheometer, an instrument that can measure the way in which a gel or liquid flows in response to an applied force. There are two types of rheometer which vary in accordance to the type of stress applied [42]. The first, the extensional rheometer, applies an extensional stress to the sample. The second, the shear rheometer applies a shear stress to the sample, i.e. the force vector component of the stress is parallel to the cross section of the material. For this study, the latter will be used.

In terms of the quantitative analysis, it was the elastic modulus,  $G'$ , of the gels which was of greatest interest. The elastic modulus of a material is a quantitative description of its tendency to undergo elastic deformation upon the application of a force [43]. Generally stiffer materials have a higher elastic moduli.

## 2. Experimental

*Abbreviations:* nanodiamond (ND); oxidised nanodiamond (ND-OH); chlorinated nanodiamond (ND-Cl); poly (ethylene glycol) methyl ether methacrylate (PEGMA); ethylene glycol dimethacrylate (EGD); tetrahydrofuran (THF); atom transfer radical polymerisation (ATRP); round bottom flask (RBF); room temperature (RT); Fourier Transform Infrared Spectroscopy (FTIR); X-Ray Powder Diffraction (XRD); Elemental Analysis (EA); Scanning Electron Microscopy (SEM); Transmission Electron Microscopy (TEM); Dynamic Light Scattering (DLS); Raman Spectroscopy (RS).

### 2.1. Preparation and Characterisation of the Nanodiamond Starting Material

The detonation ND ( $d = 50$  nm) purchased from Microdiamant AG was suspended in water (1 wt%). The ND suspension (30 mL) was sonicated using an ultrasonic probe (100 W, VWR 150D) to break up any ND aggregates. The water was then removed by freeze drying (SciQuip, Christ Alpha, 1-2 LD) overnight to yield a dry black powder, (ND, 270 mg). The ND surface functionality was characterised using; FTIR (Perkin Elmer, Spectrum One Spectrometer), XRD (Bruker AXS D8 Advance Powder Diffractometer) and EA (Euro EA Elemental Analyser). The size and morphology of the particles were determined via SEM (JEOL FESEM 6330 FEG, JOEL JSM 5600LV SEM) and TEM (JEOL JEM 1200 EX, JEOL JEM 2010). A quantitative measure of the size was also carried out using DLS (Zetasizer Nano ZS, Malvern). -**FTIR** (neat): 3273 (b, O-H, alcohol); 1741 (m, C=O); 1622 (m, O-H, alcohol); 1436 (m, C-C); 1100 (b, O-H, alcohol); 965 (m, C-O). -**XRD**:  $2\theta = 26.2, 43.9, 62.5, 75.3, 82.6, 91.5^\circ$ . -**EA**: C 88.601, H 1.581, N 2.465, O 7.353 %. -**DLS** (water):  $d = 75.49$  nm, PDI = 0.211.

### 2.2. Nanodiamond Surface Oxidation

Purification of the ND was carried out using 'piranha solution', a mixture of  $\text{H}_2\text{SO}_4$  and  $\text{H}_2\text{O}_2$ , 3:1. To begin, the ND (270 mg) obtained in the previous step was added to a clean RBF and the conc.  $\text{H}_2\text{SO}_4$  added (15 mL, 98 %). The  $\text{H}_2\text{O}_2$  (5 mL, 30 %) was then added dropwise and the reaction mixture heated to  $60^\circ\text{C}$  for 2 h whilst stirring. Afterwards, the excess  $\text{H}_2\text{SO}_4$  was neutralised with conc. NaOH (20 mL, 97 %). Separation of the ND-OH from the remaining reaction mixture was carried out using several centrifugation, washing and redispersion cycles. The ND-OH was then freeze-dried (SciQuip, Christ Alpha, 1-2 LD), to yield a fine black powder, (ND-OH, 200 mg). The ND-OH surface functionality was characterised using; FTIR (Perkin Elmer, Spectrum One Spectrometer), XRD (Bruker AXS D8 Advance Powder Diffractometer) and EA (Euro EA Elemental Analyser). The size and morphology particles were determined via SEM (JEOL FESEM 6330 FEG, JOEL JSM 5600LV SEM) and TEM (JEOL JEM 1200 EX, JEOL JEM 2010). A quantitative measure of

the size was also carried out using DLS (Zetasizer Nano ZS, Malvern). **-FTIR** (neat): 3273 (b, O-H, alcohol); 1741 (m, C=O); 1620 (m, O-H, alcohol); 1113 (s, O-H, alcohol); 965 (m, C-O); 611 (m, C-O). **-XDR**:  $2\theta = 43.9, 62.5, 75.3, 91.5^\circ$ . **-EA**: C 85.316, H 1.284, N 1.271, O 12.129 %. **-DLS** (water):  $d = 90.73$  nm, PDI = 0.327.

### 2.3. Nanodiamond Surface Chlorination

The ND-OH (200 mg) obtained in the previous step was transferred to a clean RBF and the initiator, 2 chloropropionyl chloride (3 mL, 30.90 mmol) added under vacuum. The reaction mixture was then stirred vigorously for 24 h at RT. Afterwards any remaining initiator was removed by heating to 50 °C for 6 h under vacuum. The ND-Cl was then obtained as a fine black powder, (170 mg). The ND-Cl surface functionality was characterised using; FTIR (Perkin Elmer, Spectrum One Spectrometer) and EA (Euro EA Elemental Analyser). The size and morphology of the particles was determined via SEM (JEOL FESEM 6330 FEG, JOEL JSM 5600LV SEM) and TEM (JEOL JEM 1200 EX, JEOL JEM 2010). A quantitative measure of the size was also carried out using DLS (Zetasizer Nano ZS, Malvern). **-FTIR** (neat): 1204 (s, C=O); 1140 (s, C-O); 638 (m, C-O); 550 (m, C-Cl). **-EA**: C 85.324, H 1.277, N 1.171, O 12.134, Cl 0.094 %. **-DLS** (water):  $d = 91.46$  nm, PDI = 0.308.

## 2.4. Nanodiamond Hydrogel Synthesis

Synthesis of the nanodiamond hydrogels was carried out using a modified method of ATRP [28]. The reactions were repeated in the absence and presence of the cross-linker, EGD.

### 2.4.1. Absence of Cross-Linker

In total six reactions were carried out in the absence of the cross-linker, EGD. The quantities of the reagents required for each reaction are outlined in Table 3.

Reaction	2-chloropropionyl chloride / mg	ND-Cl / mg	ND-OH / mg
R1	0	0	0
R2	76	0	0
R3	0	0	10
R4	0	0	20
R5	0	10	0
R6	0	20	0

**Table 3:** Reagents required for the six reactions carried out in the absence of the cross-linker.

It is worth noting that for each reaction, the concentrations of the monomer, PEGMA, and the catalyst,  $[\text{Cu}(\text{I})(\text{bpy})_2\text{Cl}]$ , were constant. Conversely, the quantities of the ND-OH, ND-Cl and initiator, 2-chloropropionyl chloride, varied throughout.

To begin, the quantities of the initiator and ND outlined in Table 3, were added to each of the reaction vessels along with 5 mL of milli-Q water. The solutions were then sonicated for 1 h (100 W, VWR 150D) to break up any ND aggregates. After degassing for 2 h, the bpy ligand (211 mg, 1.08 mmol) could then be added, along with the  $\text{Cu}(\text{I})\text{Cl}$  (53 mg, 0.54 mmol) and the degassed monomer, PEGMA, (9.70 g, 23 mmol). This was carried out under nitrogen. The reaction mixtures were then stirred continuously at RT for 24 h under an inert nitrogen atmosphere. Upon the onset of polymerisation, a distinct increase in viscosity was observed. Exotherms of 5 - 10 °C were recorded also. After 24 h, the reactions were quenched by opening them to air, the colour of the solutions changed from brown to blue.

Upon successful hydrogel formation, the gel was removed from the reaction mixture and washed thoroughly with water. Characterisation of the hydrogel matrix was carried out using FTIR (Perkin Elmer, Spectrum One Spectrometer) and RS (Renishaw 2000 Laser Raman Spectrometer).

Where there was no obvious sign of hydrogel formation, the reaction products were retrieved by simple separation and extraction using THF (50 mL) and excess Mg SO<sub>4</sub> (15 g). Subsequent to Buchner filtration, the THF supernatant was then passed through a silica column to remove residual any catalyst. Removal of the THF was then carried out by rotary evaporation, 40 °C. For those reactions where ATRP took place, a white solid was observed. Primitive characterisation of the polymer products was carried out by recording their melting points.

#### 2.4.2. Presence of Cross-Linker

In total seven reactions were carried out in the presence of the cross-linker, EGD, the quantities of the reagents required for each are outlined in Table 4. In order to study how the mechanical properties of the gels could be modified, three different ratios of monomer to cross-linker were used; these were 5:1, 10:1 and 20:1. R2-R4 were then carried out using the initiator, 2-chloropropionyl chloride, (76 mg, 0.60 mmol), and R5-R7 using the ND-Cl (20 mg). The concentrations of the monomer, PEGMA, and the catalyst, [Cu(I)(bpy)<sub>2</sub>Cl], were constant throughout.

Reaction	2-chloropropionyl chloride / mg	ND-Cl / mg	Monomer: Cross-linker
R1	0	0	5:1
R2	76	0	20:1
R3	76	0	10:1
R4	76	0	5:1
R5	0	20	20:1
R6	0	20	10:1
R7	0	20	5:1

**Table 4:** Reagents required for the seven reactions carried out in the presence of the cross-linker.

In terms of experimental procedure, the reactions were carried out using the same method outlined in section 2.4.1. The only change being that upon addition of the monomer, PEGMA, the cross-linker, EGD, was added also.

## 2.5. Rheological Measurements of Hydrogels

The mechanical properties of the hydrogels were investigated using a series of measurements performed on a CVO Parallel Plate Rheometer ( $d = 20$  mm). The elastic modulus,  $G'$ , was recorded in shearing mode (amplitude sweep,  $f = 1$  rad/s).

Nanodiamond Loading of Hydrogel / mg	Monomer: Cross-linker
20	0
20	10:1
20	5:1
0	5:1

**Table 5:** Rheological tests carried out on hydrogel samples.

Due to the constraints of time, only four of the hydrogel samples prepared in sections 2.3 and 2.4 could be characterised using the rheometer, see Table 5. In preparing the samples, the hydrogels were cut into cubes of approximately  $1 \text{ cm}^3$ .

## 3. Results and Discussion

### 3.1. Characterisation of the Nanodiamond Starting Material

#### 3.1.1. Surface Functionality

In order to formulate an appropriate strategy for functionalising the surface of the nanodiamond, a preliminary form of surface characterisation was required. If successful, this would provide a detailed picture of the bonding situation on the nanodiamond surface, indicating the types of functional group present and the existence of any amorphous surface domains.

Prior to characterisation, it was anticipated that the surface of the nanodiamond would be comprised of a multitude of oxygen containing groups and an array of  $sp^2$  hybridised carbon domains, as both are characteristic of detonation nanodiamond [1]. Detonation nanodiamonds possess an oxidised surface due to the use of a water coolant in the latter stages of synthesis. The water coolant can facilitate nanodiamond surface oxidation as it forms a highly reactive species when exposed to the conditions prevailing in the reactor, i.e. high pressure and temperature. Functional groups generated on the surface include the carboxyl, hydroxyl and keto groups. The graphitic  $sp^2$  hybridised domains are not generated via oxidation however. Instead these regions are formed due to the pressure declining much more rapidly than the temperature in the reactor, thus promoting the conversion of diamond to graphite.

Upon drying the nanodiamond starting material initial characterisation was carried out using elemental analysis, see Table 6.

	<b>C</b>	<b>H</b>	<b>N</b>	<b>O</b>
Nanodiamond Starting Material	88.60	1.58	2.47	7.35

**Table 6:** Elemental composition (%) of nanodiamond starting material.

The first notable observation was the surprisingly high content of oxygen detected in the sample, in this case 7.35 %. In good agreement with the literature [6], this was indicative of the oxidised nature of nanodiamond surface comprising of a number of oxygen containing groups, i.e. OH, C=O, COOH, etc. It is worth noting that the percentage composition for oxygen was actually determined by subtraction, thus a certain degree of error could be associated with this value, i.e. if another element present in the sample remained undetected.

Traces of nitrogen were also detected, albeit comprising only 2.47 % of the overall composition. In the literature, these traces were attributed to N-V centre defects found within the lattice of the nanodiamond core. It has also been suggested that these traces could be remnants of the explosives used to produce the nanodiamond during detonation synthesis [44]. Interestingly however, there was no suggestion of any kind of nitration of the nanodiamond surface. The reason being that nitrogen containing groups are notoriously difficult to establish on the surface, even after numerous functionalisation steps [1].

The only other point to be made concerning the results of the elemental analysis is that the sample was dominated by carbon with a percentage composition of 88.60 %. This was to be expected nonetheless, with carbon constituting the bulk of the  $sp^3$  hybridised diamond core.

Following initial characterisation by means of elemental analysis, the nanodiamond starting material was characterised via FTIR to yield information regarding the types of functional group present on the nanodiamond surface. The spectrum for the nanodiamond starting material is included below, see Figure 19.

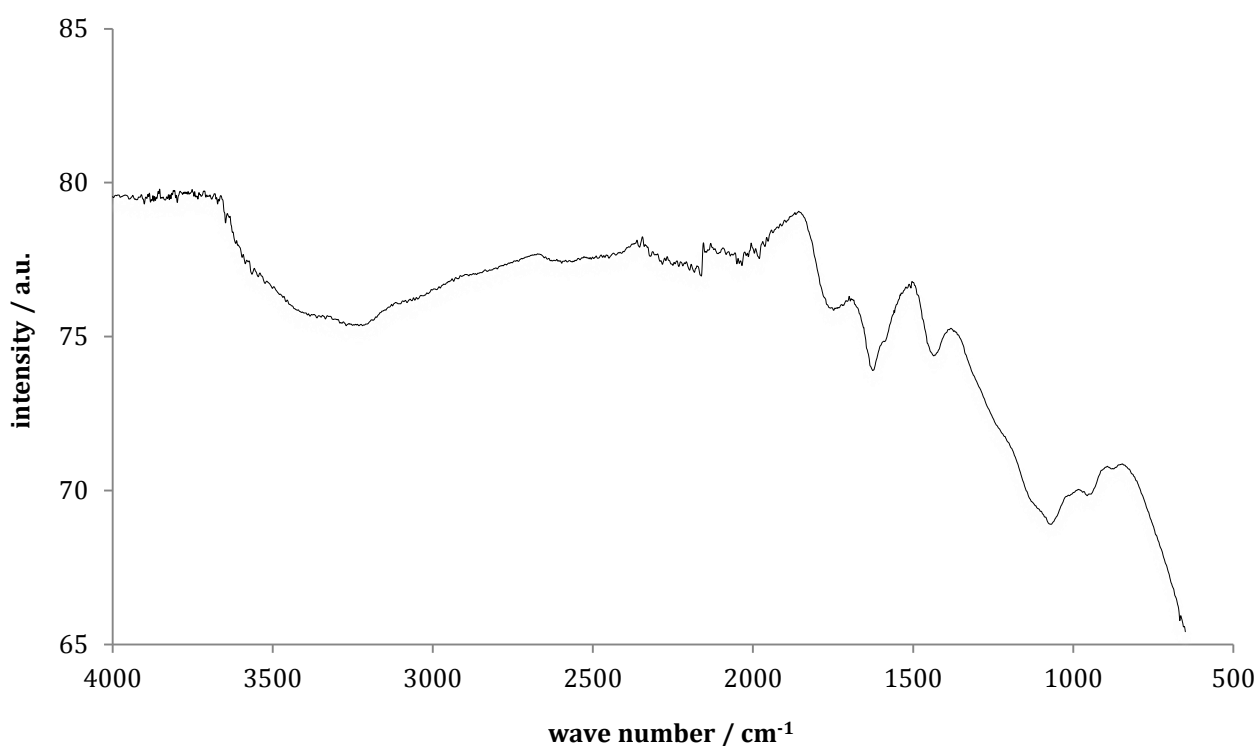


**Figure 19:** FTIR spectra of nanodiamond starting material.

The spectrum above was indicative of a number of different functional groups on the surface of the nanodiamond with each of the absorption peaks corresponding to a specific bond vibration. The broad peak at 3273  $cm^{-1}$  for example, corresponded to an O-H stretching vibration, and was thus indicative of a dense covering of hydroxyl groups on the nanodiamond surface. This was also

confirmed by the peaks at 1622 and 1100  $\text{cm}^{-1}$ , which corresponded to the O-H bending and deformation modes of the surface hydroxyl groups. Other peaks of interest include the ones at 965 and 1740  $\text{cm}^{-1}$ , which were assigned to C-O and C=O stretching vibrations respectively, again indicative of the oxidised nature of the surface. With regards to the C=O stretch, assignment could be made either to the keto or carboxyl functional groups, with both having been reported in the literature [45]. Finally, the peak at 1430  $\text{cm}^{-1}$  was of some interest, as it verified the graphitic nature of the nanodiamond outer shell, as it had arisen due to some form of unsaturated C-C bond vibration.

Thus in an attempt to further characterise the graphitic nature of the nanodiamond surface, the crystal structure of the nanodiamond was studied using X-ray powder diffraction, see Figure 20.

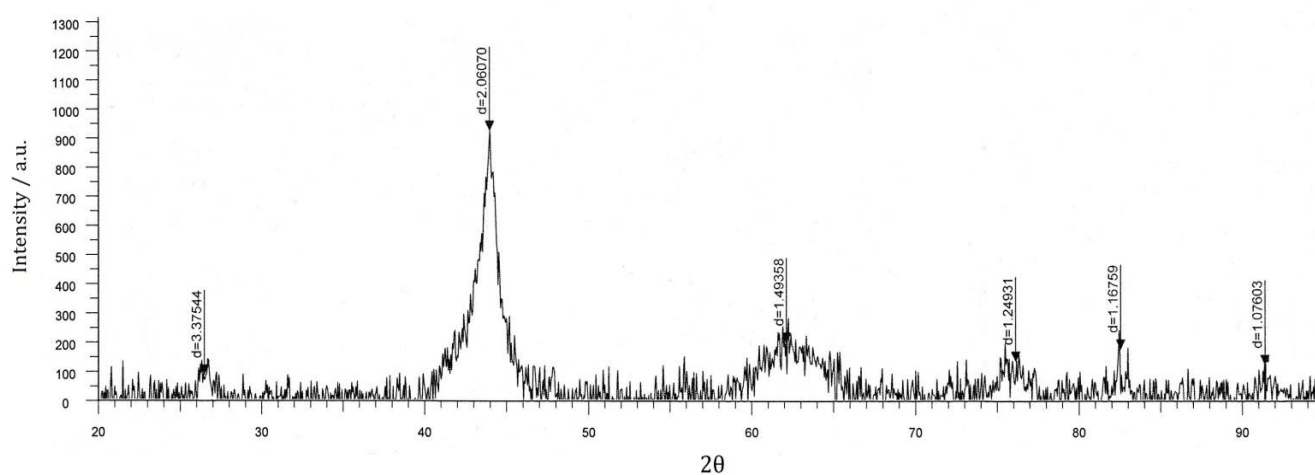


**Figure 20:** X-ray diffraction pattern for nanodiamond starting material.

The first notable observation was that the pattern above exhibited all of the classic signals one would expect for bulk diamond, with peaks at  $2\theta = 43.9, 75.3$  and  $91.5^\circ$ , corresponding to the (111), (220) and (311) planes of the diamond lattice. There was also a peak at  $2\theta = 63.5^\circ$  corresponding to the (331) plane, a feature that is only observed in the diffraction pattern for nanoscale diamond [38].

It was the additional peaks at  $2\theta = 26.2$  and  $82.6^\circ$  that were of greatest significance however, as they were indicative of the (0002) and (1120) planes of graphite [38]. Thus it was verified that some form of graphite was indeed coated on the nanodiamond surface, as first predicted.

### 3.1.2. Size

It was imperative that the size and morphology of the nanodiamond particles were subject to characterisation, as both features have been shown to have an inherent effect upon the mechanical properties of any nanodiamond composites made. Mochalin *et al* [46] for example, reported a fivefold increase in the elastic modulus of an epoxy nanodiamond composite, when the average size of the incorporated nanodiamond increased from 20 to 40 nm.

The nanodiamonds used within this study, were said to possess an average diameter of approximately 50 nm according to the specifications outlined by the supplier. Thus in order to verify this information, a quantitative measurement of the average diameter of the nanodiamond particles was carried out by means of DLS, the results for which are included in Table 7.

	Z-Average Diameter/ nm	PDI
Nanodiamond Starting Material	75.49	0.21

**Table 7:** Size and PDI of the nanodiamond starting material, recorded via DLS.

After one hour of sonication, the average size of the particles was measured to be 75.49 nm, thus a 50 % increase on the size quoted by the supplier. The reason for the discrepancy was most likely due to aggregation of the nanodiamond facilitated by hydrogen bonding between the oxygen containing functional groups on the surface of the nanodiamond. The polydispersity index, a measure of the size distribution of the nanoparticles, was also indicative of some form of aggregation. Therefore, in the future a more efficient method of nanodiamond deagglomeration would be required; this could be facilitated using a higher frequency sonicator probe for example.

Proceeding quantitative analysis, the size of and morphology of the particles were also characterised by means of SEM and TEM, see Figures 21 and 22.

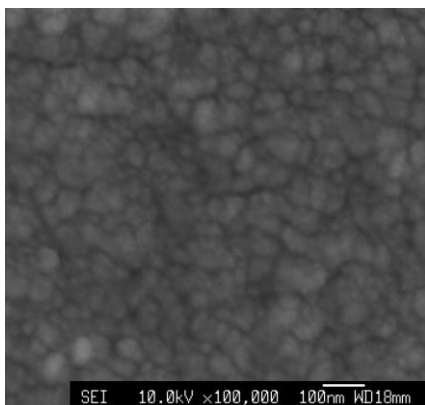


**Figure 21:** SEM micrograph of nanodiamond starting material.

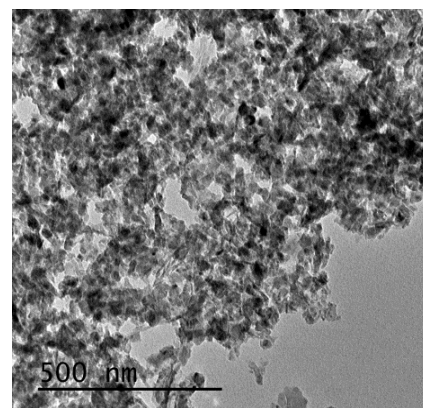


**Figure 22:** TEM micrograph of nanodiamond starting material.

Essentially, both imaging techniques indicated the size of the nanodiamond particles was somewhere within the region of 60 – 80 nm, thus complimenting the value of 75 nm obtained using DLS. Likewise, the size distribution exhibited above was quite fitting for a PDI of 0.21.

Finally in terms of morphology, the particles closely resembled those seen in the literature as reported by Turner *et al.* In this sense they were roughly spherical in shape, with what would appear to be a smooth surface.

### **3.2. The Effects of Surface Oxidation**

Characterisation of the nanodiamond starting material was indicative of a surface covering comprising a number of oxygen containing groups, and a  $sp^2$  hybridised graphitic outer shell. The oxygen containing moieties detected on the surface included the hydroxyl group and various carbonyl variants. In terms of reactivity, it was the hydroxyl group which was of greatest interest, as it would enable chlorination of the nanodiamond surface via reaction with 2-chloropropionyl chloride in a subsequent step [23]. Thus to maximise the number of hydroxyl groups on the surface of the nanodiamond, some form of oxidation was required. Two of the most effective methods for surface oxidation require thermal treatment in the air or the use of a mixture of strongly oxidising mineral acids. In this context however, it was only a variant of the latter which was deemed suitable, as oxidation of the surface was carried out using piranha solution, a 3:1 mixture of concentrated  $H_2SO_4$  and  $H_2O_2$  [21]. Piranha solution was thought to be the most appropriate choice of oxidant as it is capable of selectively hydroxylating the nanodiamond surface without carboxylation. In addition, various papers have reported how piranha solution can be used to remove any graphitic domains on the surface, thus creating a more homogeneous bonding situation for further functionalisation. Removal of the graphitic impurity is enabled as the amorphous  $sp^2$  hybridised carbon is oxidised fully to  $CO_2$ , whilst the diamond is conserved due its lower reactivity towards mineral acids. An added bonus of using piranha solution is that the concentrated  $H_2SO_4$  can remove any metallic impurities from the nanodiamond sample originating from the reactor [21].

#### **3.2.1 Surface Functionality**

Included below is the X-ray diffraction pattern for the nanodiamond sample after oxidative treatment with piranha solution, see Figure 23. Although remarkably similar, as one would expect for two samples possessing the same bulk crystal structure, there are some distinct differences between the diffraction patterns of the two samples. The main one being that the characteristic signals for graphite, observed at  $2\theta = 26.2$  and  $82.6^\circ$ , for the nanodiamond starting material, are completely absent in the diffraction pattern for the oxidised nanodiamond sample. This provides

unequivocal evidence for the effective removal of the graphitic domains on the surface of the nanodiamond upon treatment with piranha solution, as first reported by Chung *et al* [21].

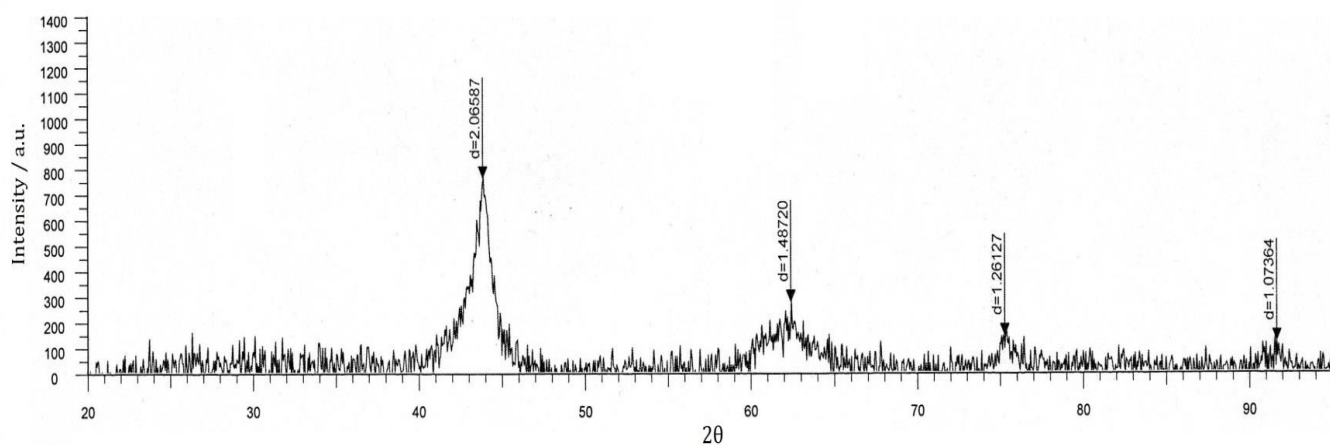


**Figure 23:** X-ray diffraction pattern for the oxidised nanodiamond.

Removal of the outer graphitic shell was also confirmed by means of FTIR, see Figure 24 for a comparison of the IR absorbance before and after oxidative treatment.

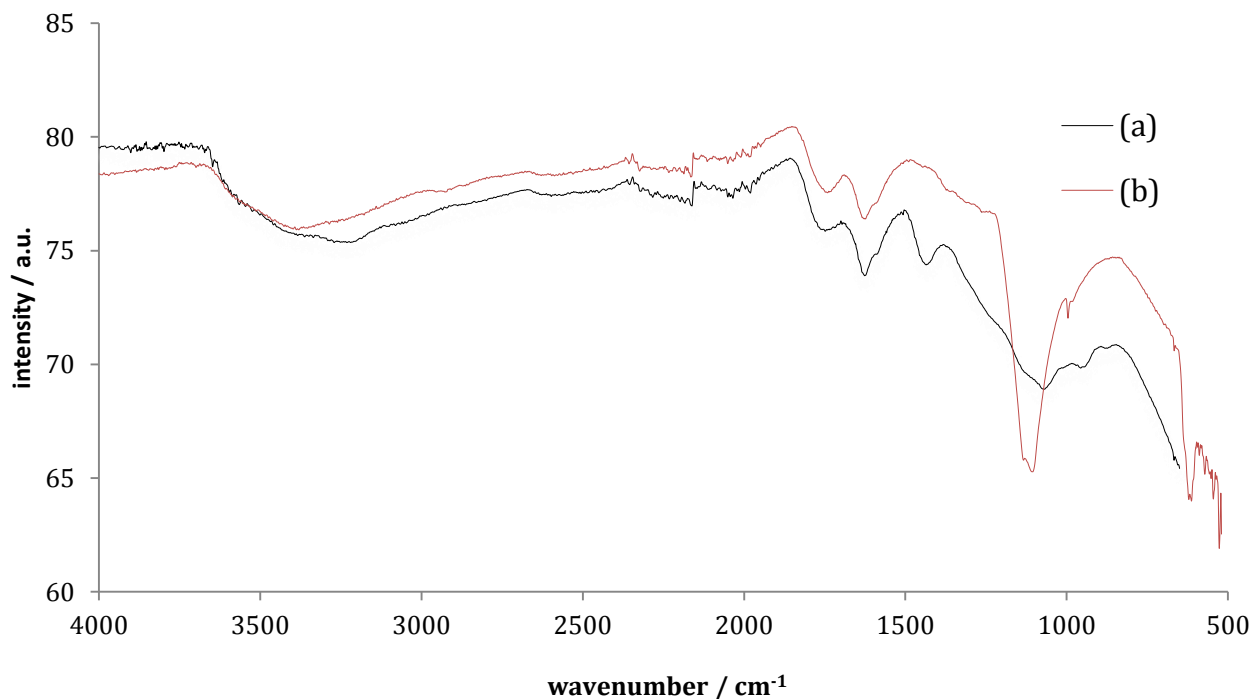


**Figure 24:** FTIR spectra of nanodiamond before (a) and after oxidation (b).

In determining successful removal of the outer graphitic shell, it was the weak absorbance at approximately 1430 cm<sup>-1</sup> that was of greatest interest, as it corresponded to the stretching frequency of the graphitic C-C bond. It is evident that upon oxidation of the nanodiamond starting

material, the absorbance at  $1430\text{ cm}^{-1}$  disappears, thus conclusive evidence of the successful removal of the graphite from the nanodiamond surface. It is also worth noting that the absorbance for the oxidised nanodiamond, exhibits sharper peaks at  $1113$  and  $611\text{ cm}^{-1}$ , corresponding to the O-H and C-O stretching motions. These changes in the intensity of the absorbance are indicative of successful hydroxylation of the nanodiamond surface, and are in good agreement with the observations reported by Loktev *et al* [48].

Interestingly however, the O-H stretch at  $3273\text{ cm}^{-1}$  displayed little change upon oxidative treatment, a trend also documented in the literature, the reason for which is widely disputed. The C=O stretch at approximately  $1740\text{ cm}^{-1}$ , also exhibited no change upon treatment with the piranha solution. This was to be expected however, and suggests carboxylation of the nanodiamond surface did not occur.

Effective oxidation of the nanodiamond surface was also verified via elemental analysis, see Table 8.

	<b>C</b>	<b>H</b>	<b>N</b>	<b>O</b>
<b>Nanodiamond Starting Material</b>	88.60	1.58	2.47	7.35
<b>Oxidised Nanodiamond</b>	85.32	1.28	1.27	12.13

**Table 8:** Elemental composition (%) of nanodiamond before and after oxidation.

Outlined above are the percentage compositions of the elements present in the nanodiamond before and after oxidation. The most significant change to have occurred has to be the dramatic increase in the oxygen content after oxidation, in this case by approximately 50 %. A similar change was also reported by Ando *et al* [49] suggesting that the experimental procedure used to oxidise the nanodiamond was sound. The only other change in the elemental composition worth mentioning is the slight decrease in the nitrogen content, in this case from 2.47 to 1.27 %. The nature of this change relates to the removal of any traces of the detonation explosives used to synthesise the nanodiamond.

### 3.2.2. Size

A quantitative measure of the size and polydispersity of the nanodiamond particles was carried out before and after oxidation, this was achieved using DLS, see Table 9.

	<b>Z-Average Diameter/ nm</b>	<b>PDI</b>
Nanodiamond Starting Material	75.49	0.21
Oxidised Nanodiamond	90.73	0.33

**Table 9:** Size and PDI of the nanodiamond before and after oxidation, recorded via DLS.

It was expected that the average size of the nanodiamond particles would decrease upon oxidative treatment due to the removal of any graphite on the surface. According to the data above, this was not the case however, as the average size of the particles actually increased upon oxidation; this was by almost 20 %. It is thought that the increase in the average size could have been due to some form of nanodiamond aggregation, as this would also explain the marked increase in the PDI after oxidation. Aggregation of the nanodiamond particles may have been encouraged by the increase in the abundance of oxygen containing groups on the surface, thus enabling the formation of more hydrogen bonds between the free particles in solution. Furthermore, the micrographs obtained via SEM and TEM, indicated a higher frequency of aggregates upon oxidation, see Figures 25 and 26.

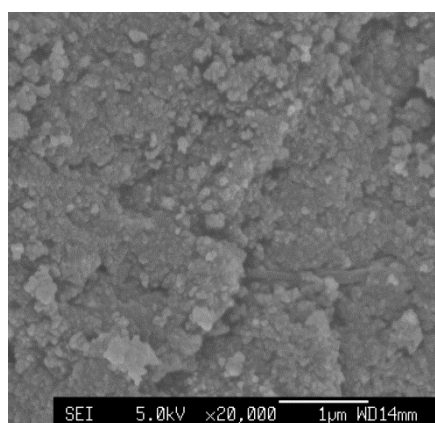


**Figure 25:** SEM micrograph of oxidised nanodiamond.

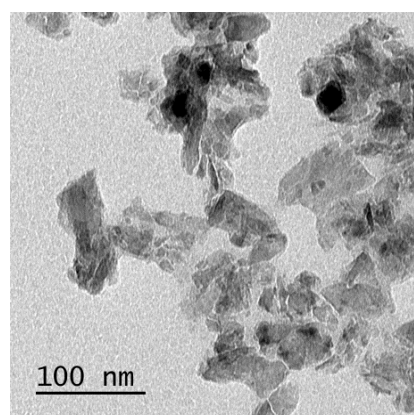
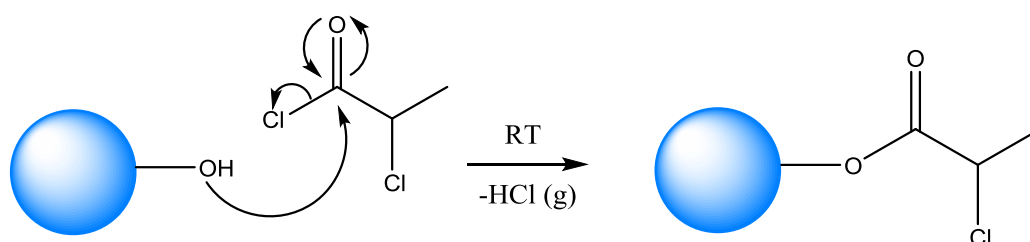


**Figure 26:** TEM micrograph of oxidised nanodiamond.

Notably, the morphology of the particles changed very little upon oxidation, despite removal of the graphitic outer shells. In this sense the particles remained roughly spherical, with a smooth surface.

### 3.3. The Effects of Surface Chlorination

Following successful hydroxylation of the nanodiamond surface, it was possible to embark upon an effective method of chlorination. The technique used within this study, first reported by Zhang et Al [23], involved reacting the hydroxyl groups on the surface of the nanodiamond with a suitable initiator, in this case 2-chloropropionyl chloride. Upon successful functionalisation, the nanodiamond would then become 'initiated', with a dense covering of chlorine atoms grafted to the surface via an array of short inert linker molecules. In this sense, the surface would be chlorinated indirectly, thus evading the issues of instability commonly associated with directly bound nanodiamond chlorine adducts. When chlorine is directly bound to the surface of the nanodiamond, i.e. without an inert linker, this instability arises due to the ease of nucleophilic attack at the site of the C-Cl bond. This bond is particularly weak, due to the capacity of the chlorine to act as a good leaving group, and due to the high stability of the tertiary carbocation left behind at the nanodiamond surface. Ultimately, this results in difficulty storing the directly bound ND-Cl adducts without compromising the chlorinated surface coverage. Thus, in order to ensure maximum retention of the chlorine on the surface, chlorination was carried out using the initiator. The reaction mechanism for the chlorination step is outlined below in Scheme 8.



**Scheme 8:** Chlorination of the surface of the nanodiamond via reaction with the initiator 2-chloropropionyl chloride.

The reaction proceeded via a second order nucleophilic substitution reaction, with the lone pair of electrons on the hydroxyl moiety having attacked the electrophilic carbon of the polar carbonyl bond of the initiator. Heterolytic cleavage of the C-Cl bond will then have followed, with the chloride generated capable of accepting a proton from the hydroxyl moiety, to form HCl, the waste product of the reaction. The initiator will have become covalently bound to the nanodiamond surface via an ester type linkage. The chlorinated nanodiamond was then capable of facilitating ATRP for hydrogel synthesis.

### 3.3.1. Surface Functionality

In order to determine whether or not successful chlorination of the nanodiamond surface had occurred, the nanodiamond was characterised by means of FTIR, see Figure 27.

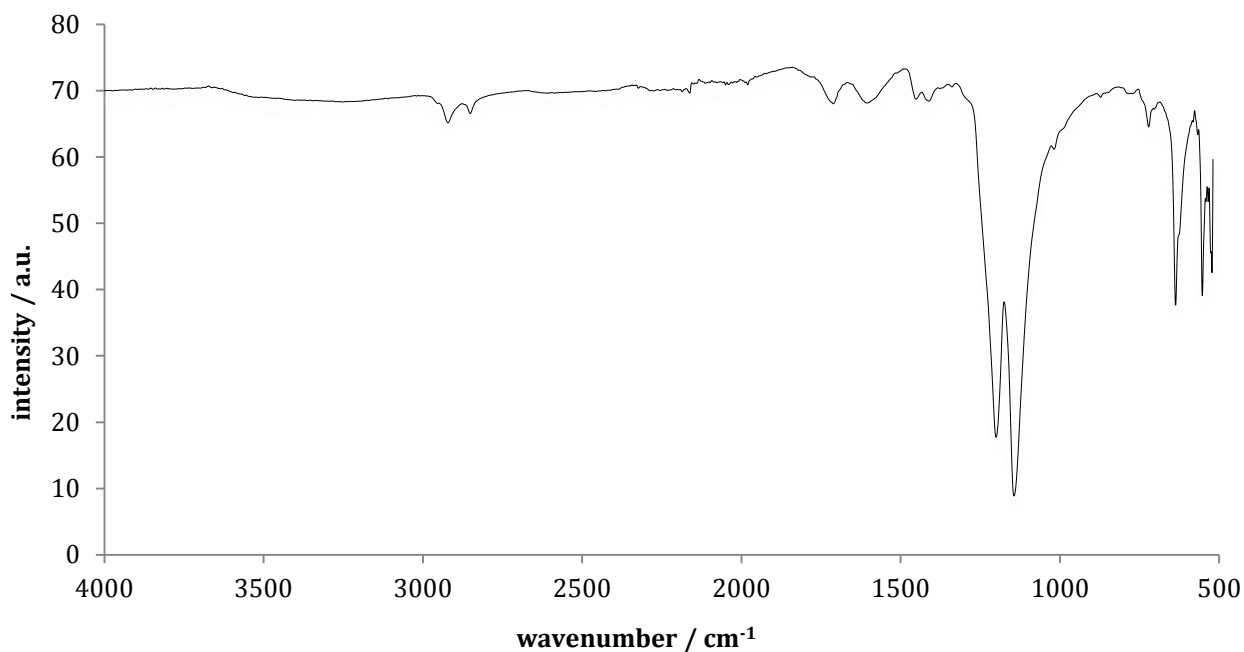


**Figure 27:** FTIR spectra of nanodiamond after chlorination.

The absorption stretch at approximately 550 cm<sup>-1</sup> is the one of greatest significance, as it corresponds to a C-Cl stretching vibration therefore it is indicative of the initiator derivative having been successfully bound to the nanodiamond surface [23]. In the same way, the sharp peaks at 1204 and 1140, also indicate successful functionalisation, as they represent the C=O and C-O bonds of the new ester type linkage. In addition, the absence of the O-H stretch near 3273 cm<sup>-1</sup>, suggests all of the hydroxyl groups on the nanodiamond surface have reacted with the initiator, to give a high conversion.

In order to substantiate the findings above, the chlorinated nanodiamond was also characterise via elemental analysis. The table below outlines the elemental compositions of the nanodiamond before and after chlorination, see Table 10.

	<b>C</b>	<b>H</b>	<b>N</b>	<b>O</b>	<b>Cl</b>
Oxidised Nanodiamond	85.32	1.28	1.27	12.13	0
Chlorinated Nanodiamond	85.32	1.28	1.17	12.13	0.09

**Table 10:** Elemental composition (%) of nanodiamond before and after chlorination.

The data above is indicative of successful chlorination, as traces of chlorine were detected in the sample after the attempted surface functionalisation. With this said, the percentage composition of chlorine detected was somewhat lower than first expected, possibly indicating only a sparse covering of chlorine on the nanodiamond surface. If true however, this would contradict what was first assumed using FTIR, in this case that the surface of the nanodiamond had been chlorinated fully. It is therefore quite likely that the percentage composition of chlorine detected in the sample was much lower than what was actually present. This could have been due to the fact that chlorine is notoriously hard to detect using elemental analysis, thus in the future a more effective method of detecting the chlorine on the surface would be required. As a final point, it is also worth noting the percentage composition of the other elements present, exhibited no change upon chlorination. This was to be expected as the bulk of the  $sp^3$  hybridised diamond core will have remained unaffected.

### 3.3.2. Size

The average size of the nanodiamond particles before and after chlorination was measured using DLS, the results for which are outlined in Table 11.

	<b>Z-Average Diameter/ nm</b>	<b>PDI</b>
Oxidised Nanodiamond	90.73	0.33
Chlorinated Nanodiamond	91.46	0.31

**Table 11:** Size and PDI of the nanodiamond before and after chlorination, recorded via DLS.

Quite simply, the average size and polydispersity of the nanodiamond particles exhibited no change upon chlorination, as expected. This was the case because the initiator molecules grafted to the surface were less than 1 nm in length such that any change in the size of the particles would have been beyond the accuracy of the instrumentation.

The chlorinated nanodiamond particles were also imaged using SEM and TEM, see Figures 28 and 29 respectively.

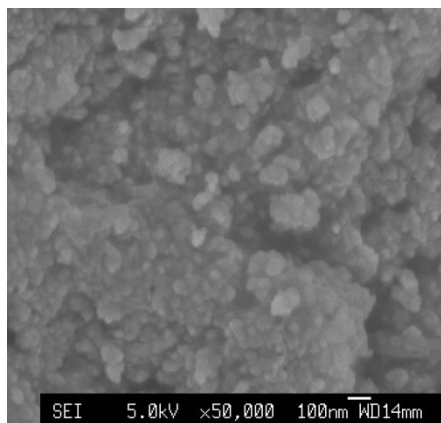


**Figure 28:** SEM micrograph of chlorinated nanodiamond.

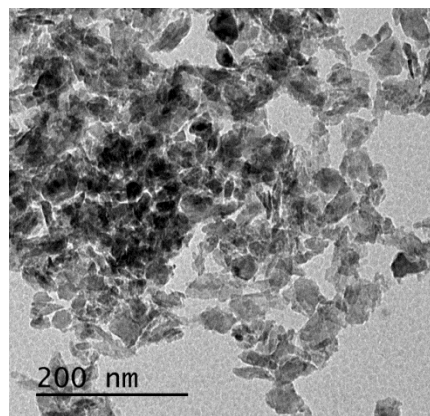


**Figure 29:** TEM micrograph of chlorinated nanodiamond.

The average size of the particles appeared to coincide with the measurements carried out using DLS. The morphology of the particles has also changed very little upon chlorination.

### 3.4. Nanodiamond Hydrogel Synthesis

Upon successful chlorination of the nanodiamond surface, it was possible to synthesise the nanodiamond hydrogel by means of ATRP [35]. The new nanodiamond composite would be comprised of an array of functionalised nanodiamond particles covalently incorporated within a three-dimensional polymer matrix, and to our knowledge would be the first of its kind reported in the literature. ATRP was used as it offers an efficient route for synthesising polymers of a well-defined molecular weight and polydispersity, thus enabling a good degree of homogeneity within the polymer matrix. The monomer selected for polymerisation, thus constituting the main component of the hydrogel, was polyethylene glycol methyl ether methacrylate, PEGMA, which in fact is a polymer itself with a number average molecular weight,  $M_n$ , of 300, see Figure 31. Of the various monomer units available, PEGMA was deemed most appropriate due its high hydrophilicity and excellent reaction kinetics for ATRP. In addition, PEGMA possesses a low cytotoxicity, a prerequisite for any future biomedical applications of the new composite. With regards to the catalyst,  $[\text{Cu(I)}(\text{bpy})_2\text{Cl}]$  was selected for use as it had been studied

comprehensively in the literature, and was said to possess a particularly high catalytic turnover frequency. Other transition metal analogues, i.e. iron, were also considered but deemed less viable due to the high affinity of Cu(I) for chlorine, thus facilitating rapid halogen abstraction. Finally, the Cu(I) and Cu(II) oxidation states are capable of interchanging rapidly, a vital requisite for ATRP.

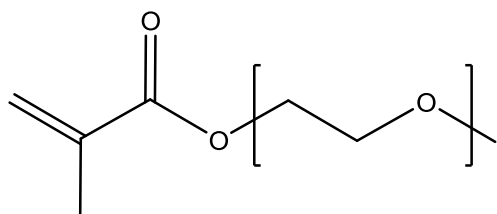


**Figure 30:** Polyethylene glycol methyl ether methacrylate, PEGMA.

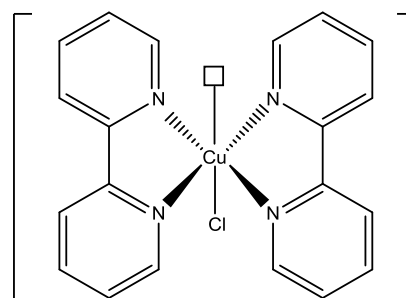
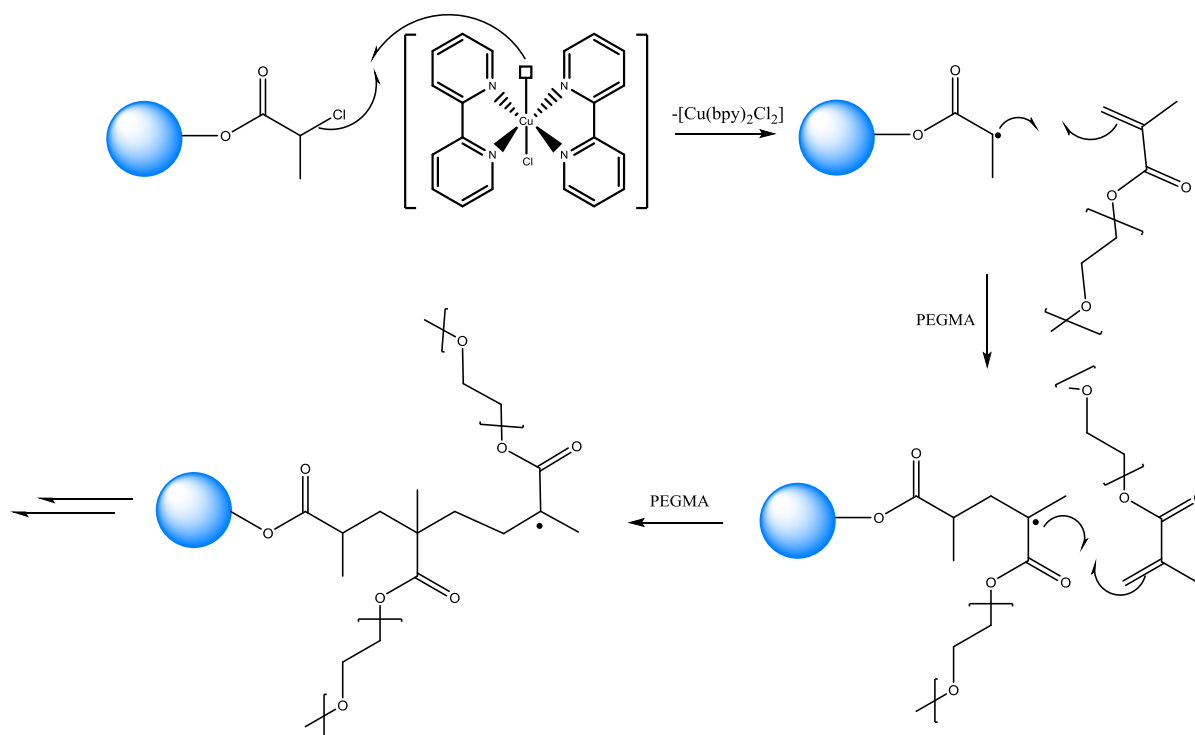


**Figure 31:**  $[Cu(I)(bpy)_2Cl]$  catalyst.

The proposed mechanism for the synthesis of the covalently incorporated nanodiamond hydrogel is included below, see Scheme 9.



**Scheme 9:** Nanodiamond hydrogel synthesis via atom transfer radical polymerisation.

The first step, the initiation step, would involve abstraction of a chlorine atom from the ‘initiated’ nanodiamond surface, to generate a reactive free radical species. Halogen abstraction would be facilitated by the  $[\text{Cu(I)(bpy)}_2\text{Cl}]$  catalyst, the driving force for which would be the formation of a stable eighteen electron octahedral  $[\text{Cu(II)(bpy)}_2\text{Cl}_2]$  complex. The radical species on the surface of the nanodiamond could then attack the vinyl bond of the monomer, PEGMA, to generate another free radical intermediate [30]. Direct chain growth at the surface would then proceed via the addition of sequential monomer units, to create a three-dimensional matrix of cross-linked polymer chains. In effect, the nanodiamonds would become tethered in all directions, thus creating a permanent, covalently cross-linked nanodiamond hydrogel.

### 3.4.1. Absence of Cross-Linker

Initially, nanodiamond hydrogel synthesis was carried out in the absence of a cross-linker to ascertain whether the chlorinated nanodiamond alone could result in sufficient cross-linking for gel formation. The details of the six reactions carried out in this step are outlined below in Table 12. It is worth noting that the monomer, PEGMA, and catalyst,  $[\text{Cu(I)(bpy)}_2\text{Cl}]$ , concentrations were constant throughout.

Reaction	2-chloropropionyl chloride / mg	ND-Cl / mg	ND-OH / mg	Observations
R1	0	0	0	No Reaction
R2	76	0	0	Polymer Formation (White Solid)
R3	0	0	10	No Reaction
R4	0	0	20	No Reaction
R5	0	10	0	Partial Nanodiamond Hydrogel Formation
R6	0	20	0	Nanodiamond Hydrogel Formation

**Table 12:** The reactions carried out in the absence of a cross-linker, and any observations made.

The first reaction to be carried out, R1, was the negative control. This reaction was carried out in the absence of any form of initiator, i.e. the 2-chloropropionyl chloride or the ‘initiated’ nanodiamond, to validate the mechanism for hydrogel synthesis, in this case via ATRP.

Essentially, if polymerisation proceeded in the absence of an initiator, one could conclude that the mechanism for polymerisation was not via ATRP, and that it went via some other route. Fortunately, this was not the case however, as polymerisation did not occur for R1, the reason being that no radical species was generated to initiate chain growth. Conversely, R2 was carried out in the presence of the initiator, 2-chloropropionyl chloride (1 equiv.), and as such it was expected that polymerisation of the monomer, PEGMA, would occur. Notably, polymerisation would not result in the formation of a hydrogel due to the absence of a cross-linker, instead it was expected that the polymer chains formed would remain free in solution. In terms of what actually took place, the reaction proceeded as expected, with a solid white polymer identified as PEGMA obtained after separation and extraction. The identity of the polymer was confirmed by measuring its melting point which was recorded at 139.5 °C, this was in good agreement with the literature value of 140 °C [50].

R3 and R4 were then carried out using the oxidised nanodiamond, yet to have been functionalised with the initiator, i.e. ND-OH. Two loadings of ND-OH were used; these were 10 and 20 mg for R3 and R4 respectively. The reactions were essentially controls, in this case testing whether or not the addition of unfunctionalised nanodiamond alone could result in polymerisation. It was expected that polymerisation would not occur for either of the reactions, as to facilitate ATRP some form of 'initiated' surface would be required. With regards to the experimental results, both reactions resulted in no polymerisation taking place as expected, thus confirming the proposed method of ATRP.

Finally, R5 and R6 were of greatest interest as they were carried out using the 'initiated' nanodiamond, i.e. the ND-Cl. As for the previous two reactions, two loadings of ND were used; these were 10 and 20 mg, for R5 and R6 respectively. It was expected that both reactions would result in nanodiamond hydrogel formation, in accordance to the mechanism proposed in Scheme 9, but also that the reaction carried out with the higher loading of ND-Cl would result in the formation of a gel with a higher elastic modulus. This was not the case however, as R5 did not result in nanodiamond hydrogel formation, instead only a slight increase in the viscosity of the solution was observed. This was indicative of polymerisation having occurred with insufficient cross-linking of the polymer chains. The lack of cross-linking will have been due to an insufficient loading of the nanodiamond, i.e. 10 mg, thus preventing the formation of a continuous gel. Conversely, nanodiamond hydrogel formation was successful for R6, when a loading of 20 mg was used for the ND-Cl. It is thought that this was due to the higher loading of ND-Cl resulting in sufficient cross-linking in the polymer matrix. The nanodiamond hydrogel (Figure 32), was comprised of a continuous bulk matrix and upon initial inspection possessed a good degree of flexibility. It is also worth noting that upon washing with water, the colour of the hydrogel leaked

out to form an almost colourless gel, see Figure 33. This was significant as it suggests any impurities found within the polymer matrix after synthesis could be removed effectively; an important consideration for biomedical applications of these gels.



**Figure 32:** Nanodiamond hydrogel before washing with water.



**Figure 33:** Nanodiamond hydrogel after washing with water.

Subsequently, the nanodiamond hydrogel was characterised by means of FTIR, see Figure 34.

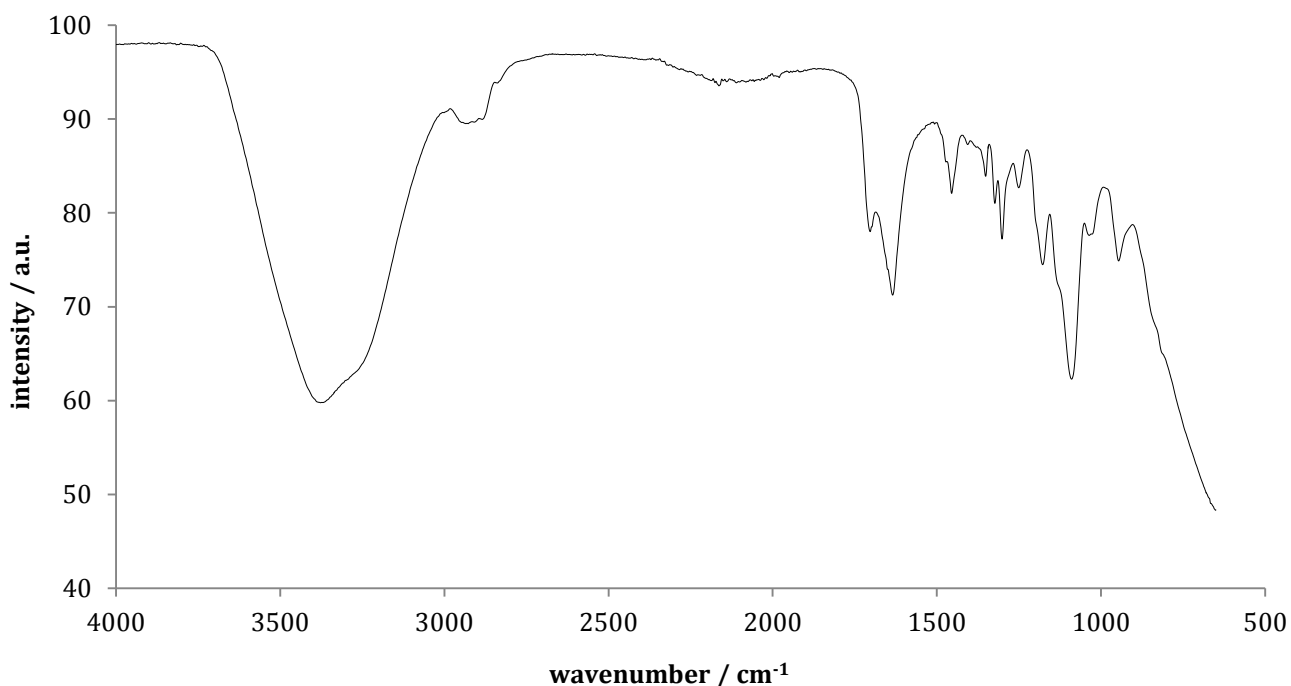


**Figure 34:** FTIR spectra of nanodiamond hydrogel.

As expected the spectra displayed a number of peaks characteristic of the PEGMA comprising the polymer matrix of the hydrogel. The two peaks of greatest interest were those at 1634 and 1090  $\text{cm}^{-1}$ , as they corresponded to the C=O and C-O stretching vibrations of the PEGMA backbone, thus confirming the chemical nature of the gel. Likewise, the broad peak at 3364  $\text{cm}^{-1}$ , was indicative

of an O-H stretching vibrations, therefore affirming the presence of water in the polymer matrix, a property ubiquitous to any hydrogel.

In order to certify that the nanodiamond had indeed been incorporated within the hydrogel, the nanodiamond composite was also characterised by means of Raman spectroscopy, see Figure 35.

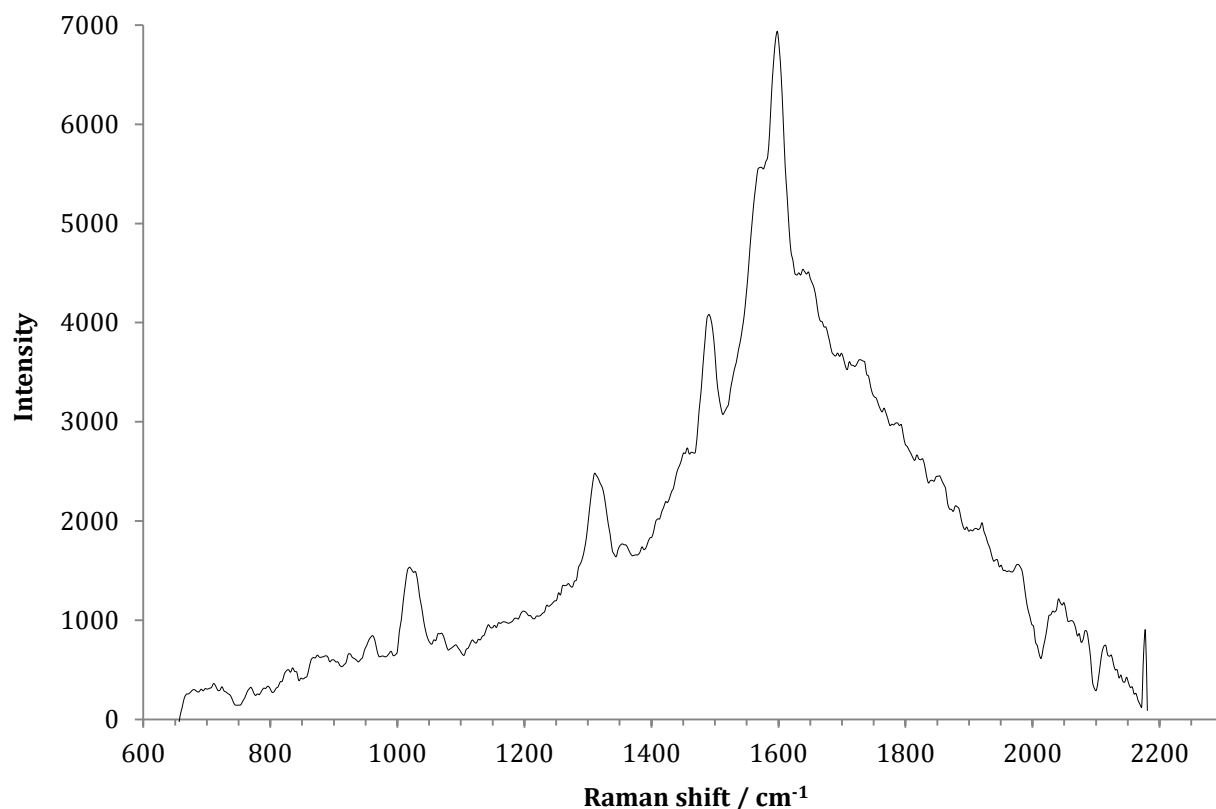


**Figure 35:** Raman spectra of nanodiamond hydrogel.

As expected, there was a well-defined peak at approximately 1332 cm<sup>-1</sup>, corresponding to a triply degenerate optical  $\Gamma$  phonon mode characteristic of diamond [3], thus confirming the successful incorporation of the nanodiamond within the hydrogel, a truly exciting result. It is worth noting however, that we cannot confirm whether or not the diamond was truly covalently incorporated within the hydrogel or simply encapsulated by means of this technique. However, if the polymerisation reaction proceeded as outlined in Scheme 9, the nanodiamond must have been incorporated covalently. In the future, it would perhaps be beneficial to image the gel by means of cryo-TEM to gain a more comprehensive understanding of the nature of the nanodiamond incorporation.

### 3.4.2. Presence of Cross-Linker

Following the synthesis outlined in the previous section, the nanodiamond composites were then prepared in the presence of a cross-linker, ethylene glycol dimethacrylate, EGD, see Figure 36. The addition of the cross-linker was to investigate how the mechanical properties of the nanodiamond hydrogels could be modified to accommodate a wider range of potential applications. The cross-linker used, EGD, was selected due to its excellent reaction kinetics towards ATRP, as well as its biocompatibility, an important consideration for any future biomedical application.

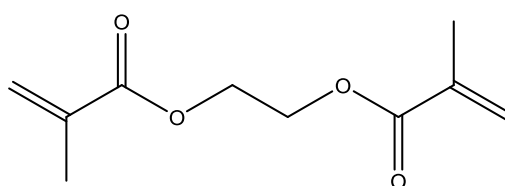


**Figure 36:** Ethylene Glycol Dimethacrylate, EGD.

In total, seven reactions were carried out using the cross-linker, the details for which are outlined below in Table 12. It is worth noting that as for the reactions described in the previous section, the monomer, PEGMA, and catalyst, [Cu(I)(bpy)<sub>2</sub>Cl], concentrations were constant throughout.

Reaction	2-chloropropionyl chloride / mg	ND-Cl / mg	Monomer: Cross-linker	Observations
<b>R1</b>	0	0	5:1	No Reaction
<b>R2</b>	76	0	20:1	Hydrogel Formation
<b>R3</b>	76	0	10:1	Hydrogel Formation
<b>R4</b>	76	0	5:1	Hydrogel Formation
<b>R5</b>	0	20	20:1	Nanodiamond Hydrogel Formation
<b>R6</b>	0	20	10:1	Nanodiamond Hydrogel Formation
<b>R7</b>	0	20	5:1	Nanodiamond Hydrogel Formation

**Table 12:** The reactions carried out in the presence of a cross-linker, and any observations

The first reaction, R1, was essentially a control carried out in the absence of any form of initiator to confirm the capacity of the EDG as a cross-linker only, i.e. that it was unable to initiate ATRP. Thus, it was expected that polymerisation would not occur, due to the absence of an initiator. This was indeed the case, as no reaction proceeded.

Conversely, R2 – R4 were then carried out in the presence of the initiator, 2-chloropropionyl chloride, in the hope of synthesising three ‘pure’ hydrogels, without nanodiamond incorporated in the polymer matrix. Three ratios of monomer to cross-linker were used; these were 20:1, 10:1 and 5:1, for R2, R3 and R4 respectively. It was expected that the hydrogels produced using the lowest ratio of monomer to cross-linker would possess the highest elastic modulus, i.e. that they would be stiffer due to a greater degree of cross-linking. In turn, when each of the reactions was carried out experimentally, hydrogel synthesis was successful throughout, with the presence of the cross-linker enabling sufficient cross-linking between the free polymer chains, creating an infinitely cross-linked three-dimensional matrix. Notably, the hydrogel synthesised using the lowest ratio of monomer to cross-linker, i.e. 5:1 in R4, appeared to have the highest rigidity as first expected.

Finally, R5 – R7 were then carried out using the initiated nanodiamond, ND-Cl, the loadings for which were 20 mg throughout. As for R2 – R4, three ratios of monomer to cross-linker were used, these were 20:1, 10:1 and 5:1 for R5, R6 and R7 respectively. It was expected that the hydrogel synthesised using the ratio of monomer to cross-linker, i.e. 5:1, would possess the highest elastic modulus. In turn, when each of the reactions was carried out experimentally, nanodiamond hydrogel synthesis was successful throughout, with the hydrogel synthesised using the lowest ratio of monomer to cross-linker appearing to be the most rigid. It is worth noting that the mechanism for hydrogel formation, i.e. via ATRP, would also be the same as described previously, the only difference being that the vinyl components of the cross-linker would also take part in the radical polymerisation.

### **3.5. Rheology of the Hydrogels**

In order to characterise the mechanical properties of the gels, a series of rheological tests was performed on the samples using a rotational CVO rheometer, an instrument that measures the way in which a gel responds to an applied force. More specifically, we were interested in measuring the elastic modulus,  $G'$ , of the gels, a quantitative measure of the tendency of a material to undergo elastic deformation upon the application of a force. In other words, the stiffer a material is, the higher its elastic modulus.

### 3.5.1. The Effect of Adding the Cross-Linker

The first series of tests were performed to determine the effect of adding a cross-linker during nanodiamond hydrogel synthesis, the results for which are outlined below in Table 13.

Monomer: Cross-linker	Elastic Modulus (G') / Pa
0	63.63
10:1	75.30
5:1	230.96

**Table 13:** The elastic modulus of three nanodiamond hydrogels prepared using three different ratios of monomer to cross-linker.

As expected there was a significant increase in the elastic modulus of the gels when the amount of cross-linker added during synthesis was increased. For example, the nanodiamond hydrogel prepared using the 5:1 monomer to cross-linker ratio, possessed an elastic modulus of 230.96 Pa, approximately three and a half times greater than the value recorded for the gel synthesised in the absence of the cross-linker. This stark difference in the elastic modulus will have been due to a higher degree of cross-linking in the gel synthesised using the EGD, which will have resulted in a decreased flexibility, i.e. a lower tendency to deform elastically when a force is applied. Interestingly, however, the relationship between the amount of cross-linker added and the elastic modulus of the gels was not linear as first expected, i.e. when the amount of cross-linker added was doubled, the elastic modulus increased by a factor of three.

To further investigate the relationship between the ratio of monomer to cross-linker and the elastic modulus of the gels, it would be necessary to test the mechanical properties of a number of additional samples. In turn, this would yield a more comprehensive set of data, meaning that any trends observed would be far more valid. It was only possible to measure the effect of the cross-linker on the mechanical properties of three nanodiamond hydrogel samples this was due to the constraints of time. As such any conclusions founded upon this data, possess a limited validity due to the high weighting of each data point.

### 3.5.2. The Effect of Adding the Nanodiamond

Perhaps of greatest interest was a comparison of the mechanical properties of the hydrogels before and after covalent incorporation of the nanodiamond. We question what, if any, differences would be observed by covalently incorporating nanodiamond into the polymer matrix. For a comparison of the elastic modulus of the hydrogels before and after covalent incorporation of the nanodiamond, see Table 14. It is worth noting that that it was only possible to conduct measurements on those samples prepared using the 5:1 monomer to cross-linker ratio, this was due to the constraints of time.

Material	Elastic Modulus (G') / Pa
Nanodiamond Hydrogel	230.96
Hydrogel	865.89

**Table 14:** The elastic modulus of two gels synthesised using a monomer to cross-linker ratio of 5:1. One of the gels consists of covalently incorporated nanodiamond.

Surprisingly, the results were contradictory to our initial hypothesis, the covalent incorporation of the nanodiamond did not confer mechanical reinforcement, but had the opposite effect. For these samples, it was apparent that the nanodiamond resulted in some form of weakening of the gel, with the elastic modulus, approximately four times smaller for the nanodiamond composite. It is possible that this could have been due to an inhomogeneous distribution of the nanodiamond in the polymer matrix of the gel, although to study this effect further, the gels would have to be imaged using cryo-TEM. More specifically, the gels would need to be frozen and sliced into infinitely thin segments, all of which could then be imaged via TEM. With this said, there are a number of other variables that may influenced the elastic modulus of the hydrogel samples, i.e. the granularity of the gels or their water content. With regards to the water content, both of the samples were prepared using 5 mL of water, therefore one would expect it to be the same for both. However, to verify this in the future, it would be necessary to record the dry mass of the gels, thus enabling one to calculate the content of water in each sample.

Notably, to improve the validity of these conclusions, it would be essential to repeat the tests on the gels synthesised using the other ratios of monomer to cross-linker. A comparison of the elastic

modulus for just two samples limits the reliability of the conclusions made, as just one piece of anomalous data could change the entire trend observed for the data.

## **4. Conclusions**

The method devised for synthesising the covalently incorporated nanodiamond hydrogels was a definite success, and as such is a cause of great excitement, especially when one considers the array of potential applications associated with this entirely new class of composite material.

In this work, it was demonstrated that treatment with piranha solution is an effective method of nanodiamond surface oxidation, particularly if one wishes to increase the abundance of hydroxyl groups on the nanodiamond surface whilst ensuring complete removal of any traces of graphite. Similarly, it was shown that reaction of the hydroxyl groups on the surface, with the initiator 2-chloropropionyl chloride, represents an efficient method of nanodiamond surface chlorination. Atom transfer radical polymerisation also proved to be an effective route for incorporating the nanodiamond covalently within the PEGMA polymer matrix, both in the absence and presence of the cross-linker, EGD. A quantitative analysis of the mechanical properties of the hydrogels was pursued also, this required carrying out a series of rheological tests. The elastic modulus was greatest for those gels prepared using the highest ratio of monomer to cross-linker, this was due to more effective crosslinking within the polymer matrix. Surprisingly however, the elastic modulus of the composites decreased upon covalent incorporation of the nanodiamond, i.e. the nanodiamond did not confer mechanical reinforcement as suggested in the literature [3]. This may have been due to an inhomogeneous distribution of nanodiamond within the polymer matrix, although further study would be required to verify this.

## **5. Future Study**

### **5.1. The Effect of Nanodiamond Loading**

As seen in section 3.4.1. synthesis of the nanodiamond hydrogel was pursued using two different loadings of nanodiamond, a preliminary attempt at determining the effect of nanodiamond loading on the mechanical properties of the composites made. This is of particular interest, as when fully understood it could facilitate effective control of the mechanical properties of the nanodiamond composites. Thus, in order to further investigate this effect, synthesis of the hydrogels could be repeated using a variety of nanodiamond loadings, i.e. at 40, 60, 80 or 100 mg. The elastic modulus of the gels could then be measured using the rheological tests, outlined in section 3.5. One would expect those gels synthesised using the highest loadings of nanodiamond,

to possess the largest elastic modulus. In a similar manner, one could also investigate the effects of nanodiamond particle size on the mechanical properties of the gels.

## 5.2. The Effects of Surface Functionalisation

It would also be interesting to evaluate how the methods of surface functionalisation used throughout the project could be modified to effect the mechanical properties of the nanodiamond hydrogels. For example, instead of using piranha solution for the oxidation of the nanodiamond surface, an alternative method could be used. In this case, oxidation could be carried out using Fenton reagent, a mixture of  $H_2O_2$  and  $FeSO_4$ , first reported by *Garcia et al.* [51]. A more efficient hydroxylation of the surface could influence the mechanical properties of the gels as it would enable a denser covering of chlorine to be established on the surface of the nanodiamond, hence there would be more sites for cross-linking during ATRP.

## 5.3. Further Characterisation

In the future, it would also be worthwhile to further investigate the chemical and physical properties associated with the nanodiamond hydrogels. A more in-depth study of the mechanical properties would be of particular interest, especially regarding the effects of the covalent incorporation of the nanodiamond. To pursue this area of inquiry, it would be necessary to compare the elastic modulus of a wide selection of hydrogels before and after covalent incorporation of the nanodiamond.

As mentioned previously, it would also be beneficial to image the nanodiamond composites using cryo-TEM, to provide a detailed picture of the nature of the nanodiamond hydrogel interface.

## 6. References

- [1] Krueger, A., Lang, D., *Adv. Funct. Mater.*, **2012**, 22, 890 -906.
- [2] DeCarli, P., Jamieson, J., *Science*, **1961**, 133, 1821 – 1822.
- [3] Kreuger, A., *Carbon Materials and Nanotechnology*, 1<sup>st</sup> Edition, **2010**, 329 – 388.
- [4] Olga A., Turner, S., *J. Phys. Chem. C*, **2011**, 115, 14014 – 14024.
- [5] Dolmatov V. Y., *Russ. Chem. Rev.*, **2007**, 76, 339 – 360.
- [6] Dolmatov, V. Y., *J. Super. Mater.*, **2009**, 31, 159 – 163.

- [7] Krueger, A., Stegk, J., Liang, Y., Lu, L., Jarre, G., *Langmuir*, **2008**, 24, 4200 – 4204.
- [8] Jiang, T., Xu, S., *J. Chem. Soc.*, **1996**, 92, 3401 – 3406.
- [9] Kovalenko, I., Bucknall, D. G., Yushin, G., *Adv. Funct. Mater.*, **2010**, 20, 3976 – 3986.
- [10] Parthasarathy, M., Klingenberg, D., *J. Mater. Sci. Eng.*, **1996**, 17, 57 – 58.
- [11] Treloar, L. R., *Introduction to Polymer Science*, 1<sup>st</sup> Edition, **1970**, 36 – 38.
- [12] Benedek, G., *Nanostructured Carbon for Advanced Applications*, 1<sup>st</sup> Edition, **2001**, 3 -5.
- [13] Bondar, V. S., Pozdnyakova, I. O., *Phys. Solid State*, **2004**, 46, 758 – 760.
- [14] Ho, D., Man, H. B., *Phys. Status Solidi A*, **2012**, 209, 1811 – 1818.
- [15] Huang, L. C., Chang H., *Langmuir*, **2004**, 20, 5879 – 5884.
- [16] Cai P. J., Cheng C., *Langmuir*, 27, 1085 – 1091.
- [17] Chao, J., Chung, K., *Biophys. J.*, **2007**, 93, 2199 – 2208.
- [18] Ho, D., *Nanodiamonds: Applications in Biology and Medicine*, 1<sup>st</sup> Edition, **2010**, 270 – 275.
- [19] Butenko, Y., Kuznetsov, V., *Carbon Nanostruct.*, **2006**, 14, 557 – 564.
- [20] Gogotsi, Y., Osswald, S., *J. Am. Chem. Soc.*, **2006**, 128, 11635.
- [21] Chung, H., Rondin, L., *Phys. Rev. B*, **2010**, 82, 1154491 - 1154495
- [22] Khabashesku, V., Lui, Y., Margrave, J., *Chem. Mater.*, **2004**, 16, 3924 – 3930.
- [23] Zhang, X., Wei, Y., Tao, L., *Polymer*, **2012**, 53, 3178 – 3184.
- [24] Behler, K., Stravato, A., *ACS Nano*, **2009**, 3, 363 – 369.
- [25] Loh, X. J., Sherman, O. A., *Polymer and Self Assembled Hydrogels*, 1<sup>st</sup> Edition, **2013**, 1 – 40.
- [26] Carpi, A., Phillips, G., *Progress in Molecular and Environmental Bioengineering*, 1<sup>st</sup> Edition, **2011**, 117 – 138.
- [27] White, E., Yutvin, J., *J. Polymer Sci. B*, **2013**, 51, 1084 – 1099.
- [28] Matyjaszewski, K., Wang, J., *J. Am. Chem. Soc.*, **1995**, 117, 5614 – 5617.
- [29] Walton, D., Lorimer, P., *Polymers*, 2<sup>nd</sup> Edition, **2005**, 29.

- [30] Matyjaszewski, K., Xia, J., *Chem. Rev.*, **2001**, 101, 2921 – 2990.
- [31] Yu, Q., Zeng, F., Zhu, S., *Macromolecules*, **2001**, 34, 1612 – 1618.
- [32] Mironov, V., Prestwich, G., *J. Mater. Chem.*, **2007**, 17, 2054 – 2060.
- [33] Bonassar, L., Vacanti, C., *J. Cell Biochem. Suppl.*, **1998**, 31, 297–303.
- [34] Thomas, E., Kang, Y., Wallish, J., *Nat. Mater.*, **2007**, 6, 957 – 960.
- [35] Wang, X., Armes, S., *Chem. Commun.*, **1999**, 18, 1817 – 1818.
- [36] Pan, L., Yu, G., Bao, Z., *Nat. Mater.*, **2007**, 6, 957 – 960.
- [37] Clayden, J., Greeves, N., Warren, S., Wothers, P., *Organic Chemistry*, 2<sup>nd</sup> Edition, **2006**, 65 -72.
- [38] Zou, Q., Wang, M. Z., *Micro & Nano Letters*, **2009**, 4, 133 – 141.
- [39] Joy, D., *Scanning Electron Microscopy*, 1<sup>st</sup> Edition, **2006**, 1 – 20.
- [40] Williams, D. B., Carter, C. B., *Transmission Electron Microscopy*, 2<sup>nd</sup> Edition, **2009**, 1 – 8.
- [41] Berne, B. J., Pecora, R., *Dynamic Light Scattering*, 1<sup>st</sup> Edition, **2000**, 1 – 10.
- [42] Malkin, A. Y., Isayev, A. I., *Rheology: Concepts, Methods and Applications*, 1<sup>st</sup> Edition, **2006**, 1-50.
- [43] Wolfenden, A., *Dynamic Elastic Modulus Measurements*, 1<sup>st</sup> Edition, **1990**, 1 – 42.
- [44] Mitev, D., Dimitrova, R., *Diamond & Rel. Mater.*, **2007**, 16, 776 – 780.
- [45] Chung, P., Cheng, C., *J. Chem. Phys.*, **2006**, 125, 1747131 – 174715.
- [46] Mochalin, V., Gogotsi, Y., *ACS Nano*, **2011**, 5, 7494 – 7502.
- [47] Turner, S., Lebedev, D., *Adv. Func. Mat.*, **2009**, 19, 2116 – 2124.
- [48] Loktev, V., Kalinkin, A., *Carbon*, **1991**, 29, 817 – 819.
- [49] Ando, T., Sato, Y., *J. Chem. Soc.*, **1993**, 89, 749 – 750.
- [50] Braun, D., Cherdron, H., *Polymer Synthesis: Theory and Practise*, 5<sup>th</sup> Edition, **2013**, 114 – 116.
- [51] Martin, R., Garcia, H., *Chem. Mater.*, **2009**, 21, 4505 – 4514.